Crackle sounds and lung recruitment

PhD Thesis

József Tolnai

Department of Medical Physics and Informatics

University of Szeged, Hungary

2012

List of papers included in this thesis

I. Hantos, Z., J. Tolnai, T. Asztalos, F. Peták, Á. Adamicza, A. M. Alencar, A. Majumdar, B. Suki: **Acoustic evidence of airway opening during recruitment in excised dog lungs.** *J. Appl. Physiol.* 97: 592-598 (2004)

II. Peták, F., W. Habre, B. Babik, J. Tolnai, Z. Hantos: **Crackle sound recording to monitor airway closure and recruitment in ventilated pigs.** *Eur. Respir. J.* 27: 808-816 (2006)

III. Hantos, Z., Á. Adamicza, T. Janosi, M. V. Szabari, J. Tolnai, B. Suki: **Lung volumes and respiratory mechanics in elastase-induced emphysema in mice.** *J. Appl. Physiol.* 105: 1864-1872 (2008)

IV. Tolnai, J., M. V. Szabari, G. Albu, B. A. Maár, H. Parameswaran, E. Bartolák-Suki, B. Suki and Z. Hantos: **Functional and morphological assessment of early impairment of airway function in a rat model of emphysema.** *J. Appl. Physiol*. 22. Mar 2012 [Epub ahead of print] PMID: 22442024

List of papers related to the subject of this thesis

V. Alencar, A. M., Z. Hantos, F. Peták, J. Tolnai, T. Asztalos, S. Zapperi, J. S. Andrade, Jr., H. E. Stanley, B. Suki: **Scaling behavior in crackle sound during lung inflation.** *Phys. Rev. E* 60: 4659-4663 (1999)

VI. Suki, B., A. M. Alencar, J. Tolnai, T. Asztalos, F. Peták, M. K. Sujeer, K. Patel, J. Patel, H. E. Stanley, Z. Hantos: **Size distribution of recruited alveolar volumes in airway reopening.** *J. Appl. Physiol.* 89: 2030-2040 (2000)

VII. Majumdar, A., Z. Hantos, J. Tolnai, H. Parameswaran, R. S. Tepper, B. Suki: **Estimating the diameter of airways susceptible for collapse using crackle sound.** *J. Appl. Physiol.* 107: 1504-1512 (2009)

Table of contents

List of figures and tables

Glossary of abbreviations

ΔV . . . volume increment

ΔT . . . time interval

ΔE . . . sound energy changes

η . . . tissue hysteresivity

ARDS . . acute respiratory distress syndrome

COPD . . chronic obstructive pulmonary disease

D_b . . . bronchial diameter

ERV . . . expiratory reserve volume

FOT . . . forced oscillation technique

FRC . . . functional residual capacity

G . . . constant-phase tissue damping

H . . . constant-phase tissue elastance

HF . . . high-frequency

I . . . inertance

I_{aw} . . . airway inertance

IC . . . inspiratory capacity

IU . . . international unit

iv . . . intravenous

LF . . . low-frequency

LFOT. . . low-frequency forced oscillation technique

Mch . . . methacholine

N_C . . . number of crackles

N_S . . . number of septal attachments

P_1 . . . lateral pressure at the outlet of the tube

P_2 . . . lateral pressure at the inlet of the tube

P_b . . . bronchial perimeter

P_{box} . . . plethysmograph (box) pressure

P_L . . . transpulmonary pressure

P_{rs} . . . transrespiratory pressure

P_{tl} . . . translobar pressure

P_{tr} . . . tracheal pressure

PEEP . . . positive end-expiratory pressure

PPE . . . porcine pancreatic elastase

P–V . . . pressure–volume

RV . . . residual volume

R_{aw} . . . airway resistance

TGV . . . thoracic gas volume

TLC . . . total lung capacity

T_w . . . wall thickness

V . . . volume

V_L . . . lung volume

$V(t)$ . . . inflation volume

$\dot{V}$ . . . flow

Z . . . input mechanical impedance

Z_L . . . pulmonary input impedance

Z_{rs} . . . impedance of the total respiratory system

1. Introduction

In various respiratory diseases, but also in the normal lung, respiration can be associated with acoustic phenomena. Depending on their dominant acoustic properties, the lung sounds are conventionally classified into the main categories of discontinuous (rales or crackles) and continuous sounds (wheezes and rhonchi); depending on the anatomical locus of the sound generation, tracheal, bronchial, bronchovesicular and vesicular sounds are distinguished [8, 9]. Lung sounds are usually detected by auscultation on the chest surface; hence, the acoustic events occurring in the adjacent peripheral region and passing through the local pulmonary and chest wall tissues of highly variable acoustic attenuation are preferentially sensed. Indeed, in clinical practice, the expression “breath sounds” usually means the respiratory noise heard through the stethoscope on the chest wall [10]. These sounds therefore relate to the specific peripheral area, in contrast with the sounds that can be recorded at the airway opening and are transmitted from the source through a gaseous medium of high, uniform acoustic conductance to the entrance of the airway tree. Apart from some studies on turbulent noises generated in the large airways [10], the latter measurement approach has not been utilized in investigations of lung sounds; moreover, crackles are rarely considered audible at the mouth. The present thesis includes measurements made in experimental animals with sound recordings at the airway opening, and concentrates on a single type of acoustic event, crackles. Special emphasis is placed on the association of crackles with the development of the pressure–volume (P–V) characteristics of the lungs.

1.1. Crackles

Investigations on crackling sounds date back to the invention of the stethoscope by Laënnec in 1819 [11]. Forgacs [8] proposed that crackles are associated with the sudden opening of closed airways. Crackles can be of low or high pitch and loud or faint (depending on the properties of the individual oscillatory waveform) and profuse or scanty (as they appear sequentially); other characteristics, such as the timing and appearance in the breathing cycle are also of clinical significance [9]. Crackles are associated with a number of pulmonary diseases, such as fibrosis, asbestosis, bronchiectasis, chronic obstructive pulmonary disease (COPD), pneumonia and sarcoidosis [10, 12-15], and their above-mentioned acoustic properties can be widely different and qualitatively characteristic of the disease. However, the

mechanisms involved in the generation of crackles may simply concern the separation of the adhering walls of the bronchi of different size and liquid layer thickness.

When the lungs deflate to low *V*, many peripheral airways may be closed by a liquid bridge forming between the collapsed airway walls. During slow inflation of the lungs, closed airways suddenly reopen to the accompaniment of short transient explosive sounds. The spectral content of these sounds has been analysed from recordings made on the chest surface, which probably explains why the frequency spectrum of crackles is thought to be between 200 and 2000 Hz [9].

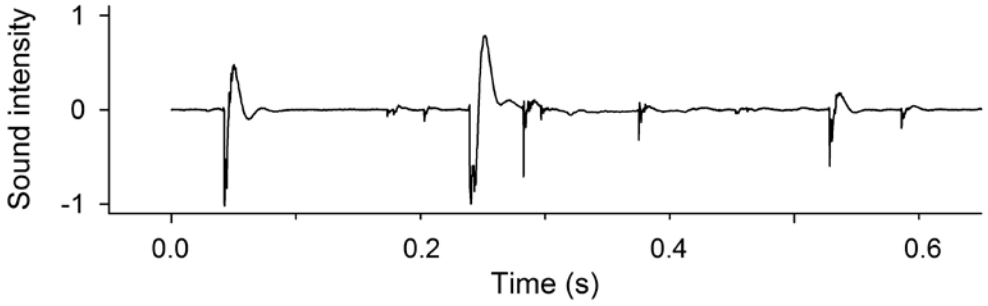

Fig. 1: A short segment of a crackle sound *P* recording in an isolated dog lung lobe.

However, a crackle recorded in the central airway consists of a sharp initial (negative) deflection in *P*, followed by an acoustic after-ring (Fig. 1). Whereas the latter involves a low-frequency (LF) oscillatory decay, most probably determined by the size of the conduits between the origin of the reopening and the recording site, the sharp transient must characterize the instantaneous wall detachment and has a wide frequency content far in excess of 2 kHz. The intensity of the initial transient is determined by the size of the reopening bronchial segment and is also influenced by the number of attenuating bifurcations it travels across. Overall, the recording of crackles at the airway opening results in high-quality waveforms that permit a better assessment of the underlying mechanisms. Although crackle sounds have been studied extensively *in vitro* in collapsed lungs [1, 5, 16], the potential of acoustic measurements for the detection of airway recruitment *in vivo* has not yet been exploited.

1.2. Lung recruitment and the *P–V* relationship

The survival rate of patients mechanically ventilated during an attack of the acute respiratory distress syndrome (ARDS) can be significantly improved if the ventilation strategy

is based on some assessment of the mechanical condition of the respiratory system [17, 18]. The lower and upper knees in the *P*–*V* curve of the respiratory system have been used to optimize the positive end-expiratory pressure (PEEP) and tidal *V* during mechanical ventilation. With the "open lung" approach [19], the PEEP is set slightly above the pressure at the lower knee of the *P*–*V* curve to minimize alveolar collapse at end expiration. Animal studies also suggest that the repetitive collapse and reopening at low airway *P*s can lead to injury due to the high shear stresses on the airway and alveolar walls [20]. Thus, an understanding of the mechanisms influencing recruitment and how they contribute to the formation of the lower knee in the *P*–*V* curve is essential if the risk of injury propagation in the lung is to be minimized.

In the normal lung, the lower knee is present in the inspiratory *P*–*V* curve exists only if the inflation proceeds from the collapsed state [16]. However, in animal models of the ARDS [16, 21] and in human subjects with the ARDS [22, 23], the *P*–*V* curve often exhibits a lower knee, even though the lung is inflated from functional residual capacity (FRC). The interpretation of the lower knee in the *P*–*V* curve of the injured lung is generally the same as for the first inflation of normal lungs from the degassed state [23, 24]. However, the relation between recruitment and the lower knee is unclear because it has also been suggested that significant recruitment can occur in patients whose *P*–*V* curve does not exhibit a lower knee [25].

It is likely that multiple mechanisms contribute to the lower and upper knees in the *P*–*V* curve, including the recruitment and the mechanics of fluid-filled alveoli [26]. However, it is commonly assumed in most studies that all mechanisms governing the recruitment process occur at the alveolar level [16, 24, 27], whereas airway closure and reopening can also affect the process of recruitment [28]. Suki *et al.* [29] put forward the idea that airways open in cascades or avalanches. During inflation, a collapsed airway suddenly opens at a critical opening threshold *P*. If the threshold *P* of one or both daughter airways is smaller than the *P* in the parent airway, then one or both segments will open simultaneously with the parent. This process propagates down the airway tree, defining an avalanche of openings. On the basis of this concept, the *P*–*V* curve of the lung and its lower knee during the first inflation from the degassed state have been successfully modelled in both symmetric [30] and asymmetric [31, 32] airway tree structures.

If recruitment occurs via avalanche-like airway reopenings, then it may be reasoned that the lung volume (V_L) recruited along the *P*–*V* curve should consist of a highly irregular

sequence of discrete volume increments (ΔV). The distribution of these ΔVs, which correspond to avalanches reaching the alveoli, should follow a power law [6, 33]. Additionally, as the airway opening is also associated with crackle sound generation [5, 8, 12, 16, 28, 34] it may be expected that the density of crackles is highest near the lower knee in the *P*–*V* curve.

1.3. Airway and parenchymal determinants of recruitment

In lung diseases, different degrees of bronchoconstriction, airway collapse and parenchymal dysfunction due to surfactant damage and/or oedema formation are observed. Although these mechanisms are often intricate, the resulting lung function impairment in diseases (such as asthma, COPD, cystic fibrosis and ARDS) primarily affects the lung periphery. It is therefore essential to employ a method that provides an objective assessment of the patency of the peripheral airways.

Monitoring of the ventilator waveforms at the airway opening and the measurement of lung mechanical parameters, such as resistive and elastic properties can be used to assess pulmonary function in mechanically ventilated patients; however, these techniques provide only indirect information about the lung periphery.

The patency of the peripheral airways can be assessed qualitatively by analysing the lower knee in the static *P*–*V* curve [18, 23, 35-39]. Although the shape of the *P*–*V* curve around the lower knee depends on many factors, analysis of the *P*–*V* relationships of the respiratory system has afforded the most comprehensive data on pulmonary recruitment [18, 23, 35, 38, 39]. Quantitative analysis of the small airway function can also be accomplished by using lung-imaging techniques, such as thoracic computed tomography or magnetic resonance imaging, although performance of these investigations in a continuous bedside setting is not yet feasible. The low-frequency forced oscillation technique (LFOT) is a powerful and specific method for the separate estimation of the airway and tissue mechanical properties [11, 40, 41]. However, the LFOT can be applied during apnoeic intervals, *i.e.* under steady state conditions, and hence only the results of the recruitment or derecruitment and not the dynamics of these processes would be revealed. The closure of peripheral airways at low transpulmonary pressures (P_L) is exaggerated in the presence of bronchoconstrictor stimuli [11], and we argue that the recruitment during a subsequent reinflation would be accompanied by an increased crackle activity.

The patency of the lower airways is fundamentally maintained by the parenchymal tethering forces, and loss of elasticity in the parenchymal network would lead to increased collapsibility of the bronchi. In emphysema, which is characterized clinically by a loss of elastic recoil and significant hyperexpansion of the lungs, permanent destruction of the parenchymal structure takes place [42, 43]. Although a variety of mechanisms (protease-antiprotease imbalance, inflammation, abnormal extracellular matrix remodelling, mechanical forces, *etc.*) have been proposed to be involved in its pathogenesis, the progressive nature of emphysema is still poorly understood [44].

The physiological characterization of emphysema requires the measurement of pulmonary mechanics [45, 46]. In clinical studies, absolute V_Ls [such as the residual volume (RV), FRC and total lung capacity (TLC)] and their ratios are used to characterize emphysematous changes [47-49]. To gain an insight into the pathogenesis and progression of the human disease, various small animal models of emphysema have been developed [45, 50-53].

The animal models of emphysema commonly concentrate on the parenchymal destruction, and several studies have reported a reduction in the number of alveolar attachments around small airways [54-56]. Less attention has been paid to the possibility of airway impairment, but in general no functional loss has been observed in the airways. Indeed, the airway resistance (R_{aw}) has been reported to be similar in normal and emphysematous mice [3, 45], and baseline pulmonary resistance has been reported to return to the control level after 3 weeks of porcine pancreatic elastase (PPE) treatment in rats [54]. However, remodelling processes following the elastolytic intervention [57] alter the bronchial wall structure, and presumably also the airway function. The net effect of these structural changes on airway mechanics is basically unclear, but it may be anticipated that both the overall resistance of the airway tree and the stability of the bronchial wall, as reflected by the reopening processes, are affected by the emphysematous changes.

2. Aims and hypotheses of the present thesis

The overall aims of this thesis were to measure and analyse the acoustic events of lung reopening as indicators of the pre-existing derecruitment state, and to interpret the crackles as markers of the discrete events of the development of the pulmonary *P–V* diagram (as opposed to continuous elastic distension) during slow inflations. The specific aims and hypotheses were as follows.

First, we hypothesized that the process of recruitment and the lower knee in the *P–V* curve in the normal lung are mainly determined by avalanche-like airway reopenings rather than simple alveolar recruitments. We expected that the density of crackles is highest around the lower knee in the *P–V* curve, because the opening of the airways is also associated with crackle sound generation. We further assumed that reinflation crackles would accompany the discrete ΔV changes. To this end, *ex vivo* studies were conducted on dog lung lobes (Study 1), which ensured the highest sensitivities both in crackle recording and in reinflation airflow measurement.

Second, we assumed that reinflation crackles sensitively characterize the preceding derecruitment state of the lungs which is determined both by the end-expiratory lung *V* and the constriction of the airways to be reopened. In order to validate this assumption, experiments were designed in mechanically ventilated open-chest pigs, with different levels of end-expiratory P_L and methacholine (Mch) doses applied prior to the slow reinflations (Study 2).

Third, we hypothesized that alterations in the parenchymal support of the airways are manifested in the airway wall stability, and hence the reinflation dynamics from very low lung *V* differ in health and experimental emphysema. We therefore set out to investigate the crackle intensity as a marker of airway reopening during slow inflations in normal and PPE-treated animals: in mice (Study 3) from the RV and in rats (Study 4) from the *in vivo* degassed state. We were also interested in whether PPE treatment causes pure parenchymal destruction or whether it also involves airway abnormalities.

3. Methods

3.1. General methodology

3.1.1. Impedance measurements

The input mechanical impedance (Z) of the lungs (Z_L) or the respiratory system (Z_{rs}) was measured with the LFOT. Because of the small size of the animals in Study 3 and Study 4, the wave tube technique (which is more accurate in the estimation of the input impedance of small structures) was selected. Z was calculated as

$$Z=Z_0\text{sh}(\gamma L)/[(P_1/P_2)-\text{ch}(\gamma L)]$$

where Z_0 and γ are the characteristic impedance and wave number of the tube, respectively, L is the tube length, and P_1 and P_2 are the lateral pressures at the outlet and inlet of the tube, respectively [58, 59].

The airway and parenchymal mechanical properties were separated by fitting the constant-phase model [40] to the Z spectra. The model consists of an airway compartment containing R_{aw} and I_{aw} (airway inertance), and a constant-phase tissue unit characterized by damping (G) and elastance (H):

$$Z=R_{aw}+j\omega I_{aw}+(G-jH)/\omega^{\alpha}$$

where j is the imaginary unit, ω is the angular frequency ($2\pi f$) and α is ($2/\pi$) arctan (H/G). R_{aw} includes all Newtonian (*i.e.* frequency-independent) resistance components.

3.1.2. Recording of tracheal sounds

A commercial miniature microphone (5×5 mm) was suspended in the lobar bronchus in dogs and in the tracheal tube in pigs (Study 1 and Study 2). In mice and rats, a metal tube (a truncated 16G or 18G needle) was attached to the microphone and positioned in front of the tracheal cannula (Study 3 and Study 4).

The electrical signal of the microphone was preamplified with a low-noise custom-made amplifier and led to the sound card of the computer used for the acquisition of the other physiological signals. The sound signal was digitized with 16-bit resolution and a sampling rate of 22.050 Hz. The recordings were made during slow inflations from the collapsed state in excised dog lung lobes (Study 1), from PEEP levels of 1 and 4 hPa in pigs (Study 2), from

the RV in mice (Study 3) and from the *in vivo* degassed state in rats (Study 4) to the TLC (30-35 hPa). In dog lobes, mice and rats, the inflations were performed with negative pressure ramps generated by a vacuum source or membrane pump in the plethysmograph; the pig lungs were reinflated via the trachea from a compressed air source. Acoustic filters were employed in the vacuum or pressure line to minimize the fluctuations in the reinflation. In order to collect more acoustic events and assess the reproducibility of the reopenings, the manoeuvres were repeated usually 2 or more times in the same condition in each animal. The duration of inflation [~20-45 s (60-120 s in dog lobes)] was selected so that the temporal resolution was sufficiently high for the identification of the individual crackles. The signals of the transrespiratory (or translobar) P and central flow ($\dot{V}$) were recorded, and the inflation volume [V(t)] was obtained by integration of $\dot{V}$.

3.1.3. Identification of crackles

The *in vivo* raw sound recordings were first high-pass-filtered at 2 kHz with a sound editor (GoldWave™ v5.12, St. John's, NFLD, Canada), in order to suppress the strong cardiogenic sound and enhance the sharp initial transients of the crackles (the *ex vivo* recordings were processed differently; see section 3.2.1). The high-frequency (HF) waveforms provided an increased temporal resolution for identification of the successive crackles, which often overlapped and hence were inseparable in the unfiltered signals. As shown in Fig. 2, although the cardiac signal largely masked the crackles in the raw recording, the high-pass filtering diminished this noise.

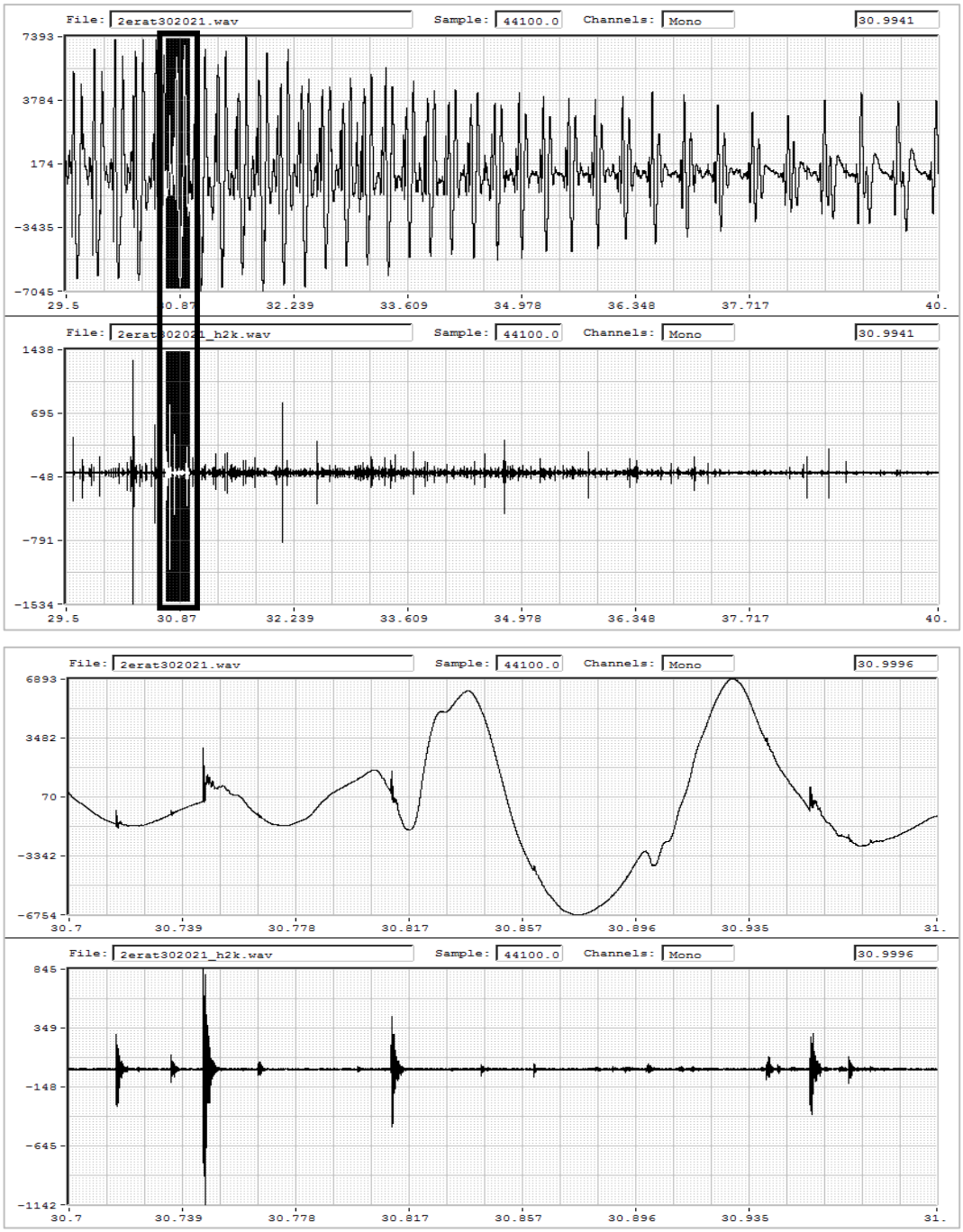

Fig. 2: A 10-s sound recording during inflation from the degassed state before and after 2-kHz high-pass filtering (top). The large-amplitude ringings and the high-frequency crackle transients are visualized by the expansion of the highlighted 0.3-s segment (bottom).

After this pre-processing, the maximum levels of background noise were estimated in each recording from the baseline and the end-inflation segments that were free of crackles, and a threshold was determined for the minimum crackle amplitude. The recordings were then divided into short (*e.g.* 0.33-ms) intervals (ΔT), and the sound energy (ΔE_i) was computed for each interval (Fig. 3). A crackle was defined as occurring when the increase in ΔE in two

successive intervals exceeded a preset value $\Lambda = \Delta E_{i+1}/\Delta E_i$; any further increase in ΔE was then checked ($\Delta E_{i+2}>\Delta E_{i+1}$, *etc.*) and the crackle amplitude was identified as the highest-magnitude sample in the last interval of the increasing ΔE sequence. On the basis of preliminary identification trials with auditory controls of the unfiltered recordings, the settings ΔT = 0.33 ms and Λ = 3 were found to provide the most reliable crackle identification results, *i.e.* the lowest numbers of missed and falsely identified acoustic events.

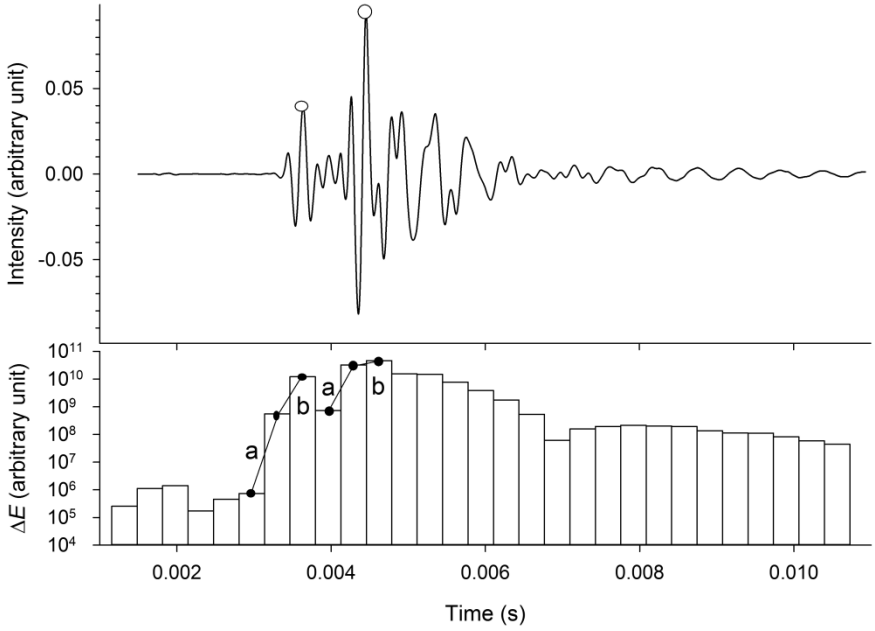

Fig. 3: A short segment of a sound recording with superimposing crackles to illustrate the method of identification of the location and amplitude of crackles. Top: sound intensity; bottom: sound energy (ΔE) calculated for successive 0.33-ms intervals. A crackle is identified when the increase in ΔE between two successive intervals exceeds a predetermined value (a); if there is a further increase, the crackle amplitude is taken as the extreme value in the next interval (b).

3.2. Study-specific methods

3.2.1. Acoustic evidence of airway opening during recruitment (Study 1)

Diaphragmatic lung lobes (n=12) were isolated from 6 mongrel dogs. The animals were anaesthetized with pentobarbital sodium (30 mg·kg^{-1}), heparinized (5,000 U) and exsanguinated through a femoral artery catheter. The procedure was approved by the Institutional Animal Care and Use Committees of the University of Szeged and Boston University. After thoracotomy, the lungs were removed, and the diaphragmatic lobes were separated and cannulated in the main bronchus. Prior to the inflation manoeuvre, the lobe was suspended in a 30-l glass box, with the bronchial cannula led to the atmosphere through a

high-resistance (6.5 hPa·l^{-1}·s) screen pneumotachograph measuring $\dot{V}$ with high precision by means of a Validyne MP-45 (±2 hPa) differential pressure transducer.

The translobar pressure P_{tl} (the difference between the airway opening and box pressures), was measured with another Validyne MP-45 (±30 hPa) transducer (Validyne Inc., Northridge, CA, USA). During the measurement, pressure was slowly increased from 0 to 30 hPa in 60-120 s by decreasing the box pressure (P_{box}) with a membrane pump (model MP 03Ez, Otto Huber, Germany). The signals of $\dot{V}$ and P were low-pass filtered at 50 Hz and sampled at a rate of 256 Hz by the analogue-digital board of a personal computer.

A 5-mm diameter microphone was introduced through the sidearm of the cannula in the main bronchus. The main techniques of sound recording and processing are described in detail in sections 3.1.2 and 3.1.3. The LF energy content of the crackles was obtained by digital low-pass filtering at 60 Hz and squaring the sound pressure amplitude. After the first inflation from the collapsed state, the box was opened to atmosphere, and the lobe was kept at $P_{tl} = 0$ for at least 5 min. The first inflation was followed by a second inflation of those lobes ($n = 7$) which did not leak during the first manoeuvre, *i.e.*, $\dot{V}$ approached zero at high P values.

The crackles were often accompanied by transients in the corresponding raw $\dot{V}$ signal (Fig. 4), which returned either to the same or to a somewhat higher level than before the transient. The signals of $\dot{V}$ were integrated to obtain V, and were also processed to identify the discrete ΔVs corresponding to the transient spikes in $\dot{V}$. Whenever the successive $\dot{V}$ transients were separable and the background noise allowed accurate identification of the beginning and end points of a $\dot{V}$ transient (this was limited to the early and late phases of inflation), ΔV was determined. For the calculation of ΔV, the post-transient level of $\dot{V}$ was taken as the baseline. To examine the relationship between recruitment and crackle sound, an energy package (ΔE_{LF}) for the duration of each identified $\dot{V}$ transient was also calculated from the LF sound data and correlated with the corresponding ΔV.

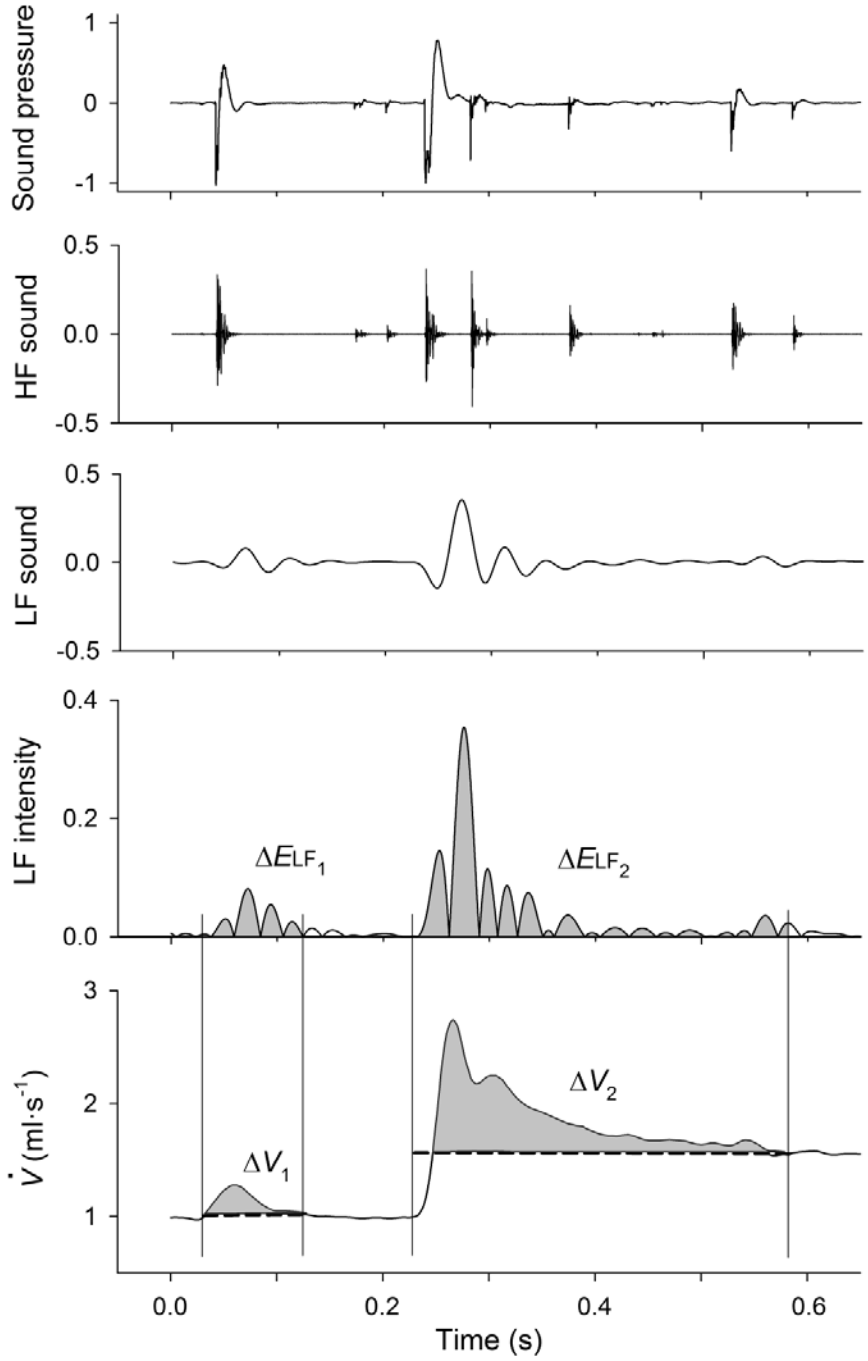

Fig. 4: A short segment of a crackle sound pressure recording, its HF (>1 kHz) and LF (<60 Hz) components, and the LF sound intensity with the corresponding flow signal ($\dot{V}$) (top to bottom, respectively) to illustrate the calculation of discrete V increments (ΔV) and associated crackle energy (ΔE). The beginning and end points of a $\dot{V}$ transient (vertical lines) and the end-transient level of flow (dashed lines) were determined visually. The shaded areas between two consecutive beginning and end points indicate the cumulated LF crackle energy (ΔE_{LF}), whereas the shaded areas above the end-transient $\dot{V}$ provide the cumulated $\dot{V}$ (ΔV). ΔE_{LF1} and ΔV_1 correspond to a single crackle, whereas ΔE_{LF2} and ΔV_2 cover several crackles whose $\dot{V}$ transients superimpose and are difficult to separate.

3.2.2. Crackle recording to monitor recruitment in bronchoconstriction (Study 2)

After approval had been granted by the Ethics and the Animal Care Committees of the Canton of Geneva (Geneva, Switzerland), 6 adult mini-pigs (17-25 kg) were studied in the supine position. The animals were anaesthetized by the inhalation of sevoflurane (up to 5%) until an intravenous (*iv*) line was secured into the ear; thiopentone (10 $mg \cdot kg^{-1}$) was then injected *iv*. The mini-pigs were next tracheotomized with a polyethylene cannula (6.5 mm internal diameter (ID); Portex, Hythe, UK) and mechanically ventilated (Model 900C; Siemens-Elema, Solna, Sweden) with a tidal volume of 7-10 $ml \cdot kg^{-1}$ at a frequency of 15 min^{-1} and an inspired O_2 fraction of 0.3 in air. A continuous infusion of fentanyl (10 $\mu g \cdot kg^{-1} \cdot h^{-1}$) via the ear vein was maintained throughout the study to ensure adequate analgesia. Anaesthesia was maintained by the *iv* injection of thiopentone (5 $mg \cdot kg^{-1}$) every 45-60 min. The carotid artery was prepared surgically in a sterile manner and cannulated (28-gauge catheter; Braun, Melsungen, Germany) for blood sampling and continuous arterial blood pressure monitoring with a calibrated pressure transducer (model 156 PC 06-GW2; Honeywell, Zürich, Switzerland). The jugular vein was prepared in the same way as the femoral artery and cannulated for delivery of the constrictor agonist. Muscle relaxation was achieved by the *iv* administration of pancuronium (0.2 $mg \cdot kg^{-1}$). The thorax was opened by means of a midline thoracotomy following an additional *iv* bolus of fentanyl (25 $\mu g \cdot kg^{-1}$) and the ribs were widely retracted. Following chest opening, a PEEP of 4 hPa was applied.

The airway P was measured continuously with a calibrated transducer (Validyne DP 45, Validyne Inc., Northridge, CA, USA). The rectal temperature, monitored with a temperature sensor (Thermalert, model TH-8; Physitemp, Clifton, NJ, USA), was maintained at 37±0.5 °C with a heating pad (Miostar, Zürich, Switzerland). Arterial blood samples were analysed radiometrically (model 505; Acid Base Laboratory, Copenhagen, Denmark) and, if necessary, the mechanical ventilation parameters were adjusted to maintain normal gas exchange. The concentrations of O_2 and CO_2 were monitored throughout the study (Ultima™; Datex/Instrumentarium, Helsinki, Finland).

The measurement system (Fig. 5) for recordings of crackles, P_L and $\dot{V}$ during slow deep reinflations, and collection of the Z_L spectra of the lungs (the latter data are not included in the present thesis) in the mini-pigs were similar to that used previously in other mammals [1, 40]. A screen pneumotachograph (11 mm ID) was used to measure $\dot{V}$ with a differential P transducer (model 33NA002D; ICSensors, Malpitas, CA, USA). An identical P transducer was used to measure the P_{tr} with reference to atmosphere (P_L) via a catheter positioned 1-2

cm beyond the end of the endotracheal tube. The tracheal cannula was detached from the respirator at end expiration (at a PEEP of 1 or 4 hPa) and connected to a buffered compressed air source. A water column was employed for limitation of P_L to 30 hPa at the end of the reinflation.

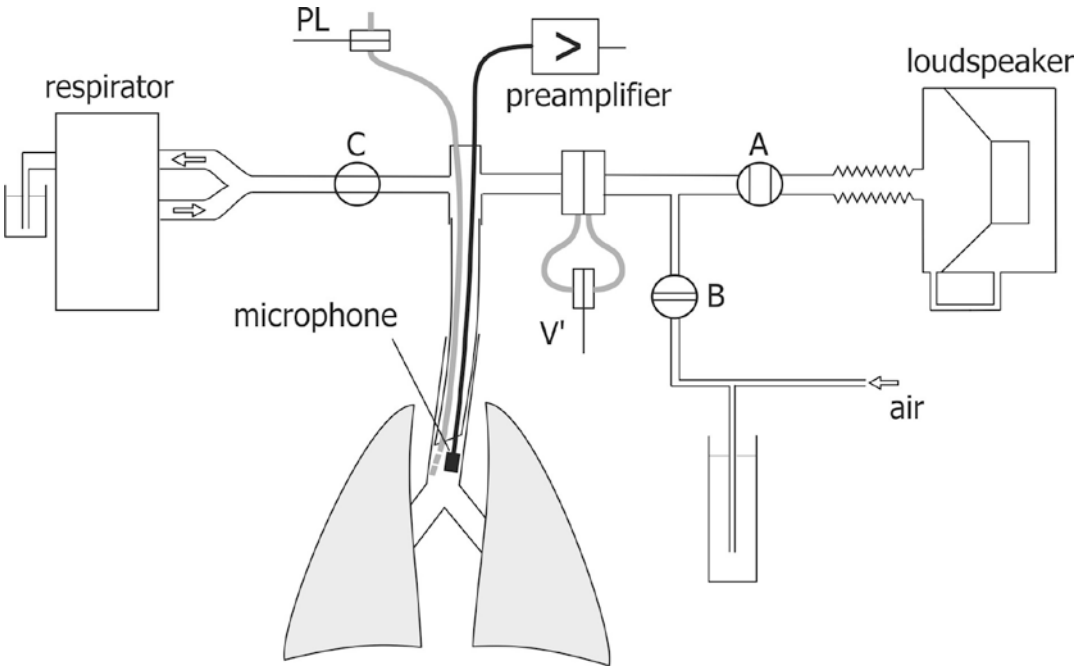

Fig. 5: Experimental set-up for the measurement of pulmonary input impedance and crackles in pigs. Taps A, B and C were adjusted according to the phases of ventilation, forced oscillation or slow inflation. P_L: transpulmonary pressure; $\dot{V}$: gas flow.

The P_L and $\dot{V}$ signals were low-pass filtered at 25 Hz and sampled with an analogue-digital board of a microcomputer at a rate of 256 Hz. The inspired $V(t)$ was obtained by numerical integration of $\dot{V}$.

The measurement and the identification of crackles were carried out as described in detail in sections 3.1.2 and 3.1.3. Figure 6 presents an example of the original sound, the high-pass-filtered sound, and the lung inflation P and V following the *iv* injection of a 40 $\mu g \cdot kg^{-1}$ Mch bolus when a PEEP of 4 hPa was maintained. It can be seen that, although the cardiac noise largely masked the crackles in the raw recording, the high-pass filtering diminished the cardiac noise in the tracheal sound recording. The majority of the crackles, including the most intense ones, appeared in the first third of the inflation.

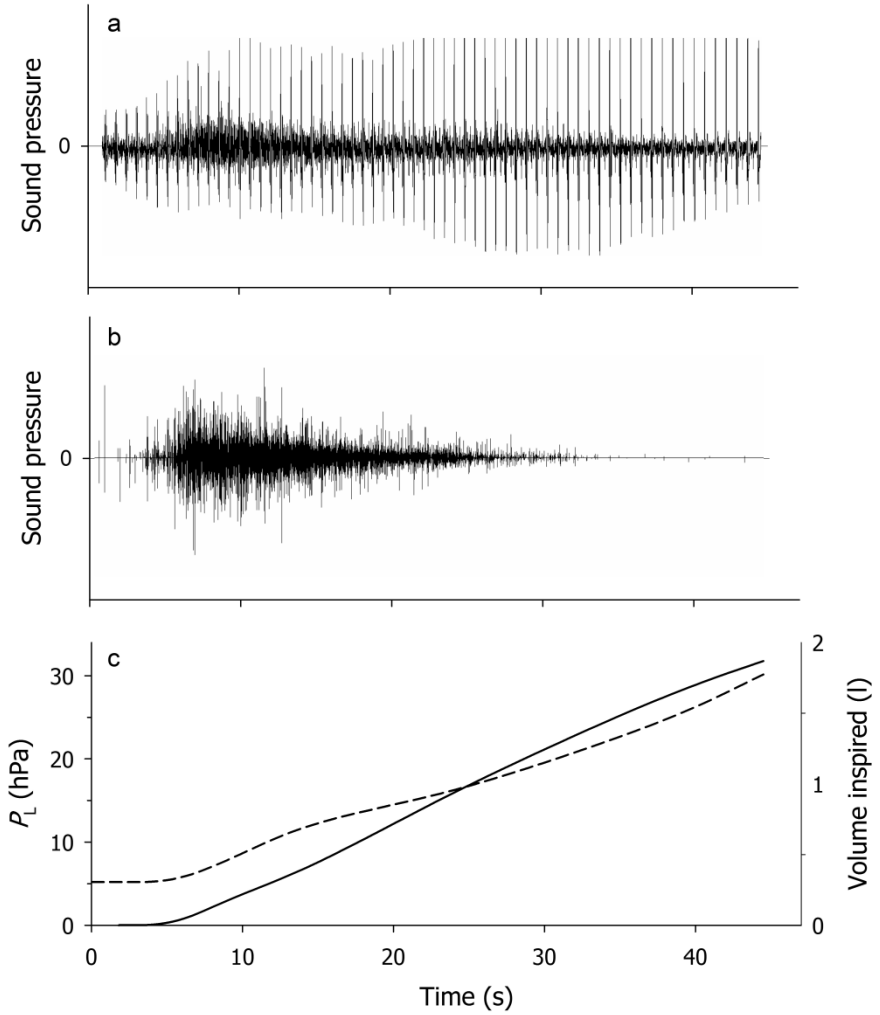

Fig. 6: Tracings of (a) the original and (b) the high-pass-filtered crackle sound pressure, with (c) the inspired V (solid) and P_L (dashed) during the inflation of a lung after an Mch challenge.

Protocol. Before the measurements, two inspiratory cycles were superimposed to standardize the volume history of the lungs. The mechanical ventilation was suspended at a PEEP level of 4 hPa, and Z_L was recorded during the resulting short (10-s) apnoeic period. Before mechanical ventilation was resumed, tap A and tap C were closed and tap B was opened (see Fig. 5), and the lungs were slowly (over ~45 s) inflated to a peak P of 30 hPa, during which period the intratracheal crackles were recorded. Following an ~2-5-min period of mechanical ventilation, the baseline Z_L and crackle measurements were repeated. Resumed mechanical ventilation was followed by the *iv* administration of a 5 $\mu g \cdot kg^{-1}$ Mch bolus. Thirty s after the injection, Z_L was measured, and immediately afterwards the lungs were inflated and the crackles were recorded. Subsequent Mch challenges were made in the same way, by administering increasing doses of Mch: 10, 20 and 40 $\mu g \cdot kg^{-1}$. After completion of the Mch challenges at a PEEP level of 4 hPa, the PEEP was decreased to 1 hPa to facilitate

lung derecruitment. The experimental procedure was then repeated while this P level was maintained during the Z_L recordings, and the subsequent inflation was also started from 1 hPa.

The number of crackles (N_C) data obtained in the two baseline recordings were averaged. The lack of mechanical ventilation between the Z_L measurement and the crackle recording guaranteed that these measurements reflected the same lung condition.

The precision of the parameters is expressed as mean±SEM. The Kolmogorov–Smirnov test was used to test data for normality. Two-way repeated measures ANOVA using a linear mixed model was used to test significance with two within-subject factors: the Mch dose and the PEEP level. In the mixed model, a composite covariance model with separate covariance structures was specified for each of the repeat factors: equal correlations were assumed for the PEEP, and a first-order autoregressive covariance structure was applied for the Mch dose. The choice of these covariance models was verified with likelihood ratio tests. For pairwise comparisons, 95% confidence intervals for the differences were computed by taking into account the significant interactions between the factors. Since N_C was not normally distributed, the changes in this parameter were tested after logarithmic transformation. The significance level was set at $p<0.05$.

3.2.3. Crackles and airway function in emphysematous mice (Study 3)

Female CBA/Ca mice were anaesthetized with an intraperitoneal injection of pentobarbital sodium (75 mg·kg^{-1}) and intubated with a 20-mm-long, 0.8-mm inner diameter polyethylene cannula under the guidance of a cold light source (model FLQ85E, Helmuth Hund, Wetzlar, Germany), according to the technique described in detail previously [60]. The PPE-treated animals received PPE (Sigma-Aldrich Hungary, Budapest, Hungary) in 50 µl of saline in one or other of two doses: 0.3 IU (n=15) and 0.6 IU (n=4) via intratracheal instillation. The control animals (n=19) received 50 µl of saline only. Three weeks thereafter, the mice were anaesthetized with an intraperitoneal injection of pentobarbital sodium (75 mg·kg^{-1}), tracheotomized, and cannulated with a 0.8-mm ID polyethylene tube. The animals were placed in the supine position in a custom-built 160-ml body plethysmograph and ventilated transmurally with a small-animal respirator (Harvard Apparatus, South Natick, MA) at a rate of 160 min^{-1}, a tidal V of 0.25 ml, and a PEEP of 2 hPa. Supplementary doses of pentobarbital sodium (15 mg·kg^{-1}) were administered as needed, generally at the beginning of the measurements. The study protocol was approved by the Institutional Animal Care and Use Committees of the University of Szeged and Boston University.

Nineteen treated animals received PPE in 50 µl of saline in one or other of two doses: 0.3 IU (n=15) and 0.6 IU (n=4) via intratracheal instillation, and 19 control mice received saline only. Three weeks thereafter, the animals were anaesthetized, tracheotomized, cannulated with a polyethylene tube, placed in the supine position in a custom-built body plethysmograph and ventilated transmurally with a small-animal respirator with a tidal volume of 0.25 ml, and a PEEP of 2 hPa (Fig. 7).

The TGV at end expiration at zero transrespiratory pressure (FRC) was measured with the plethysmographic technique [61], modified recently for the measurement of TGV in anaesthetized mice that have a weak or no respiratory effort [62]. P_{box} and tracheal pressure (P_{tr}) were measured with miniature pressure transducers (model 8507C-2, Endevco, San Juan Capistrano, CA) during stimulation of the intercostal muscles. The FRC was estimated from the P_{box} *vs* P_{tr} relationship on the basis of Boyle's principle, as detailed previously [62].

Following the measurement of the FRC, 14 control (group C1) and 14 elastase-treated mice (group E1) were used to obtain $V(t)$ and the TGV as a function of time [TGV(t) = FRC + $V(t)$]. Transrespiratory pressure (P_{rs}) was calculated as P_{tr} - P_{box}. In 5 control (group C2) and 5 treated mice (group E2), the measurement of the FRC was followed by deflation to the RV, which was accomplished by elevating P_{box} to 20 hPa; subsequently, P_{box} was lowered to -35 hPa to allow an estimate of the TLC. The box was then opened to atmosphere via a resistor to permit passive deflation. During this deflation-inflation-deflation manoeuvre, $\dot{V}$ was measured. The expiratory reserve volume (ERV) was determined by integration, and the RV was obtained as FRC - ERV.

For the measurements in groups C2 and E2, the setup was modified so that a microphone ending in a 15-mm-long, 0.7-mm outer diameter metal tube was connected to the tracheal tube adaptor of the plethysmograph (Fig. 7, inset). Tracheal sound was recorded during reinflation from the RV (P_{box} = 20 hPa) to TLC (P_{box} = -35 hPa) at a sampling rate of 44 kHz and 16-bit resolution. With stopper A closed and stopper B open, the tracheal $\dot{V}$ was measured as the pressure drop (P_{tr}) across a capillary bundle resistor while the microphone recorded the sound.

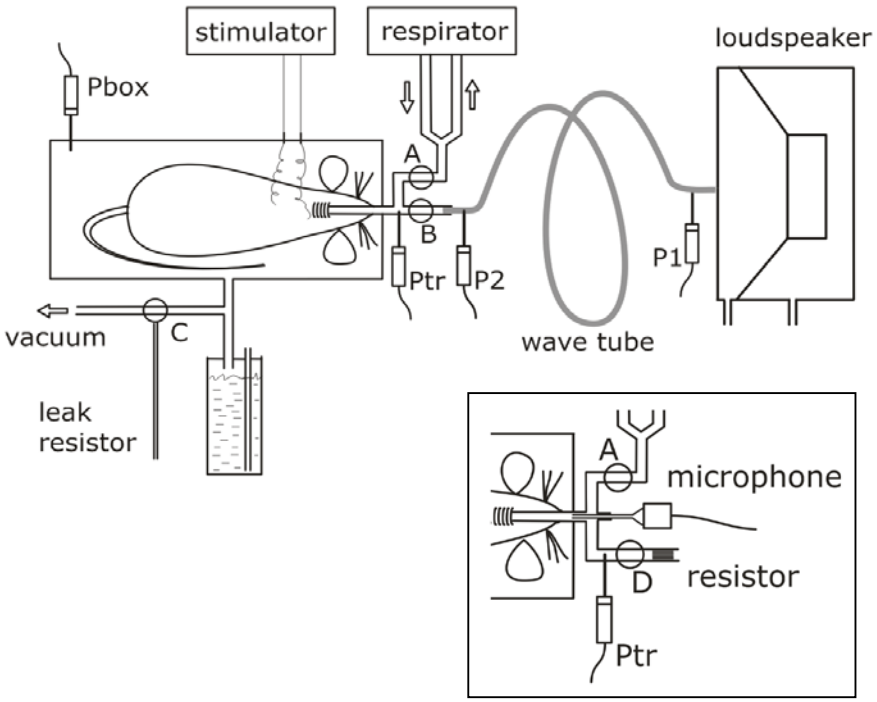

Fig. 7: Schematic arrangement for the measurement of the TGV and oscillatory mechanics. Inset: modified setup for the sound recording during VC manoeuvres.

After high-pass filtering, an 0.5-ms time window was set up and moved along the sound recording to identify the crackles (see section 3.1.3). The crackle energy was represented by its cumulative distribution, defined as the sum of the energy up to a given inflation P normalized by the total energy, whereas the crackle amplitudes were characterized with their probability density distribution.

The differences in mechanical parameters between the control and elastase-treated animals were compared by using repeated-measures ANOVA tests.

3.2.4. Crackles and airway structure/function in emphysematous rats (Study 4)

The study protocol was approved by the Institutional Animal Care and Use Committees of the University of Szeged and Boston University. Fourteen male adult (10-week-old) Sprague-Dawley rats were anaesthetized with a single intraperitoneal injection of chloral hydrate (350 $mg \cdot kg^{-1}$), intubated with a polyethylene cannula (14-gauge, Braun, Melsungen, Germany) and treated with an intratracheal instillation of 50 IU PPE (n = 8) or saline (controls, n = 6). Six weeks after the treatment, the rats were re-anaesthetized, tracheotomized, and cannulated with a 1.7-mm-ID polyethylene tube. The rats were placed in the supine position in a custom-built 2.8-l body plethysmograph and mechanically ventilated

with a small-animal respirator (Harvard Apparatus, South Natick, MA) at a rate of 80 min^{-1} and a tidal V of 8 $ml \cdot kg^{-1}$. Following the measurements, the animals were killed with an overdose of anaesthetics and the lungs were removed for histopathological evaluation.

The FRC was measured with the body plethysmographic technique [61, 62]. The inspiratory capacity (IC) and the ERV, respectively, were defined as the V changes resulting from decreasing P_{box} to -35 hPa and increasing it to 20 hPa, respectively. The TLC and RV were calculated as TLC = FRC + IC and RV = FRC - ERV.

Z_{rs} was measured with the wave tube pseudorandom forced oscillation method [59, 63], between 0.5 and 16 Hz at the FRC, during 6-s interruptions of mechanical ventilation. Constant-phase model parameters (R_{aw}, H, G and I) were estimated from 5-6 successive recordings.

Intratracheal sounds were recorded during slow (~20-s) inflations from the degassed state of the lungs to the TLC. Degassing was accomplished by 10-min ventilation with 100% O_2 and the subsequent ERV manoeuvre, followed by tracheal occlusion for 10 s; the degassing-reinflation manoeuvre was repeated 2 more times in each animal. A 15-mm metal tube (0.7-mm OD) attached to the microphone was positioned in the tracheal cannula. Sound was recorded at a sampling rate of 44 kHz with 16-bit resolution, and was high-pass filtered at 2 kHz. Individual crackle events were identified in 0.33-ms time windows. The sound recording and processing are described in detail in sections 3.1.2 and 3.1.3.

After the measurements, the rats were euthanized with an overdose of anaesthetics. The heart and lungs were removed *en bloc*, and stored in formaldehyde for 7 days before embedding in paraffin. Three transversal sections were made at 25, 50 and 75% lung height and stained for standard morphometry (haematoxylin-eosin staining; data not reported in this thesis), and with elastin and collagen.

The whole sections were scanned for the identification of bronchi suitable for further analyses with a circularity >50%. From the readings of bronchial perimeter (P_b) the diameter of an equivalent circular cross-section (D_b) was calculated. The mean wall thickness (T_w) was established from 3-4 measurements, and the number of septal attachments (N_s) was determined for each airway. The septal attachment density was calculated as N_s/P_b.

To visualize the elastin and collagen contents in the airway wall, the reliable method of Verhoeff–Van Gieson and Mason's trichrome staining were used. Quantitative analysis of the elastin and collagen densities was performed on randomly selected lung sections, using custom-made software.

The differences in lung V and mechanical parameters between the control and PPE-treated rats were compared by using Student's t-test. All the results were expressed as mean±SD. Distributions were compared by using the Kolmogorov–Smirnov test. The dependences of T_w on D_b in the two groups were tested by analysis of co-variance. A p value of less than 0.05 was considered statistically significant.

4. Results

4.1. Acoustic evidence of airway opening during recruitment (Study 1)

Representative traces of crackle sound, P_{tl} and central $\dot{V}$ during the entire recordings are shown in Fig. 8 for both the first and second inflations. In the early phase of inflation, the crackles possessed large amplitudes and were well separated from each other. As inflation continued, the density of acoustic events increased, to the accompaniment of a decrease in crackle amplitudes. In these dense intervals, the crackles became inseparable from each other in the raw recordings. P_{tl} steadily increased throughout the course of the entire inflation. The $\dot{V}$ traces consisted of a series of spikes superimposed on a slowly varying mean $\dot{V}$ level. During the first inflation, the mean $\dot{V}$ exhibited a single maximum, whereas the second inflation was characteristically biphasic, with two distinct maxima: the first rise in the mean $\dot{V}$ included massive $\dot{V}$ transients accompanied by a significant crackle activity. The mean $\dot{V}$ then decreased temporarily before a second rise, which was similar in character to that during the first inflation at the same V_L.

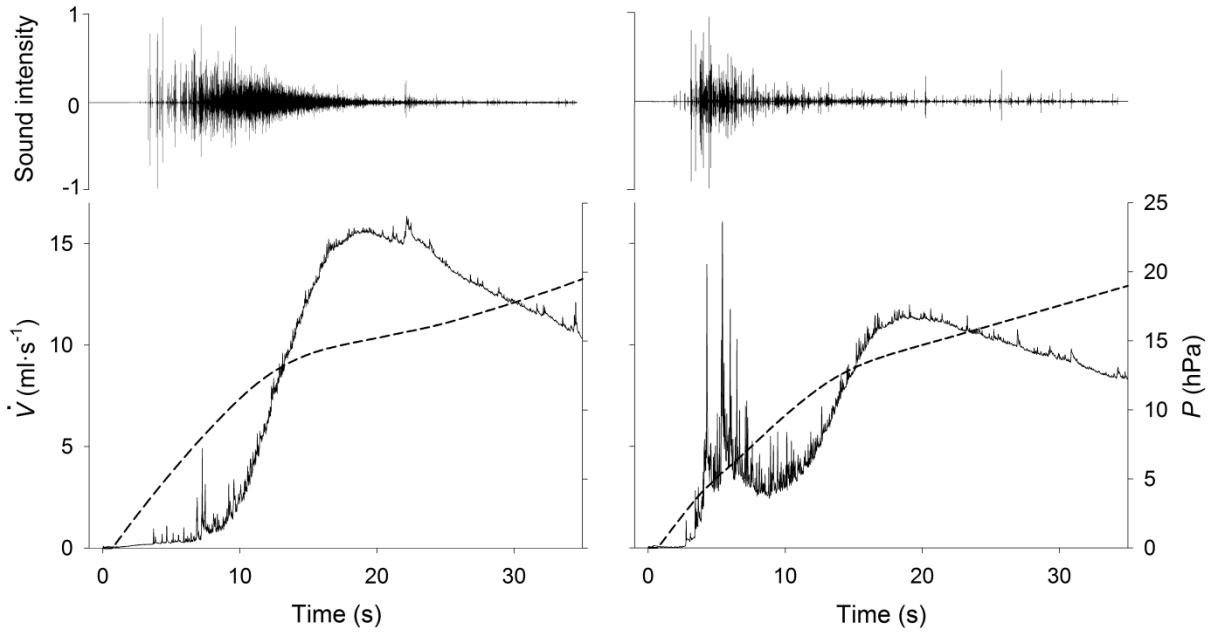

Fig. 8: Recordings of crackle sound pressure (*top*), inflation flow (*bottom*, solid lines) and P_{tl} (*bottom*, dashed lines) during the first 35 s of the first inflation (*left*) and second reinflation (*right*) of a lobe. Note the biphasic pattern and greater $\dot{V}$ transients during the second manoeuvre.

An example of the relationship between the sound energy associated with airway opening and features of the inflation *P*–*V* curves is presented in Fig. 9. During the first

inflation, the *P*–*V* curves always exhibited a single characteristic lower knee. The corresponding acoustic activity, as characterized by the values of Δ*E*, increased quickly and irregularly and remained high until a P_{tl} ~10 hPa was attained. The acoustic activity then decreased very regularly by 4 to 5 orders of magnitude, which coincided with the steep rise in *V* until the *P* reached the upper knee in the *P*–*V* curve. This was followed by another irregular pattern, during which epochs of large values of Δ*E* emerged from the low acoustic activity, indicating the occurrence of sparse, but still relatively large crackles. Although crackles were detected throughout the entire inflation process, the cumulated energy as a function of P_{tl} had reached 94-98% of its final value by the lower knee. During the second inflations, the *P*–*V* curves always exhibited two distinct lower knees, corresponding to the two maxima observed in the mean $\dot{V}$. The large values of Δ*E* during its fast rise occurred around the first knee in the *P*–*V* curve, and the increase in energy was even steeper, reaching its plateau value at much lower values of *P* than during the first inflation.

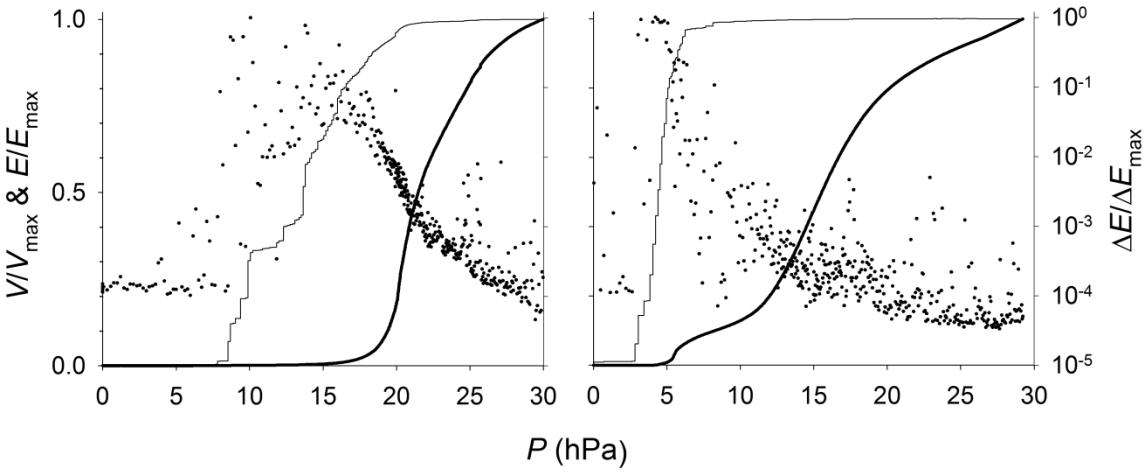

Fig. 9: Dependences of inflation volume (*V*; thick lines), sound energy calculated for successive 0.25-s intervals (Δ*E*; dots), and cumulated sound energy (*E*; thin lines), all normalized by the corresponding maximum value (V_{max}, ΔE_{max}, and E_{max}, respectively), on the P_{tl} in a lobe during the first (left) and second (right) inflation. Note the log scale for Δ*E*.

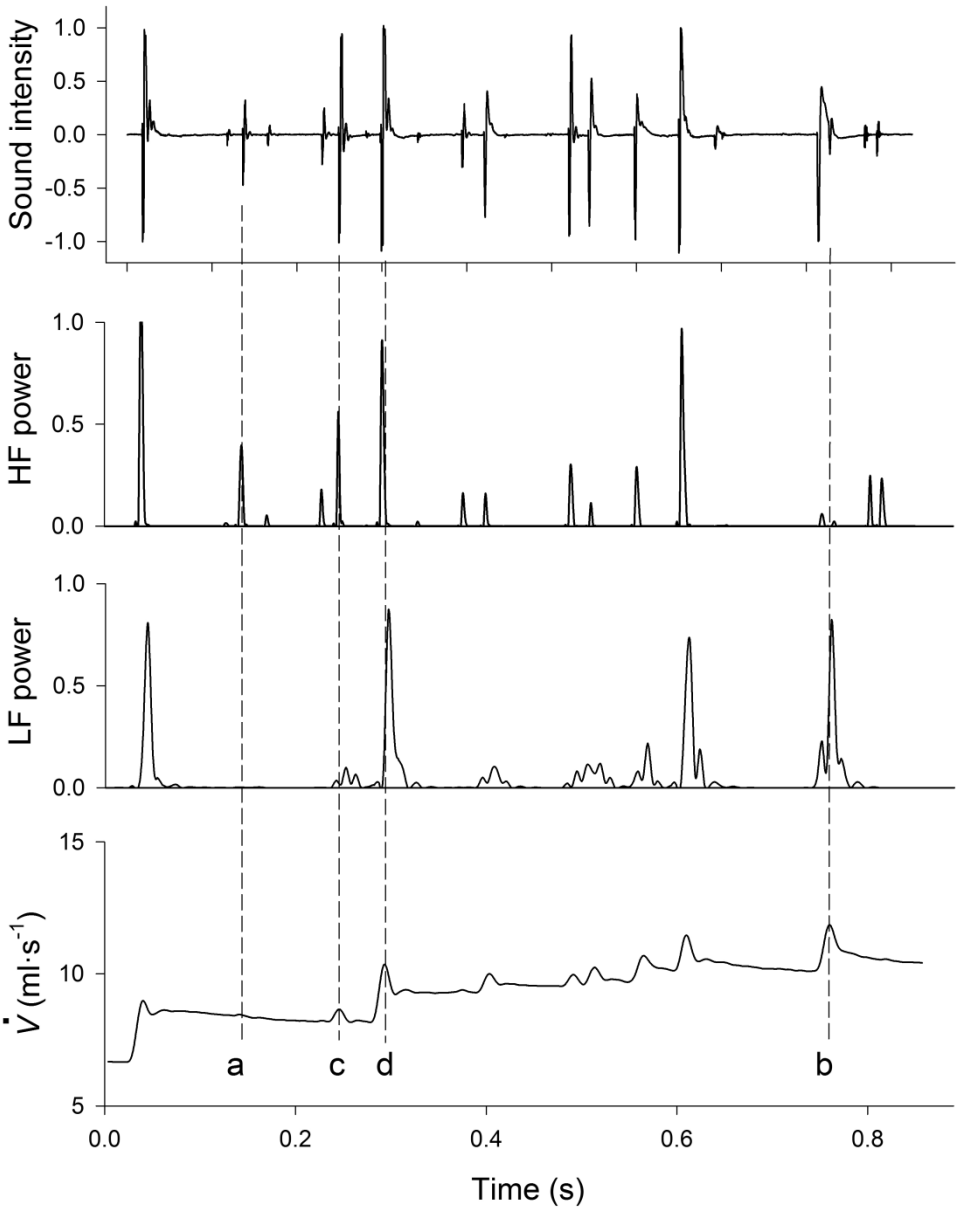

Fig. 10: A segment of a crackle (top) and $\dot{V}$ recording (bottom) during reinflation of a lobe. HF and LF sound energy data (in arbitrary units) were computed from high-pass-filtered (>1 kHz) and low-pass-filtered (<60 Hz) sound intensity, respectively. The individual crackles have different HF/LF energy contents, and the size of a transient may correlate with the HF energy (a) or the LF energy (b). Some transients are followed by increased mean flow (d), whereas others (c) are not.

When a short segment of a recording from an early phase of inflation was taken, where crackles were relatively rare and the transients were well separated (Fig. 10), the relation between crackles and transients could be examined. Every $\dot{V}$ transient was clearly marked by a crackle or a burst of crackles, whereas not every acoustic event was accompanied by a detectable transient in $\dot{V}$. It was also clear, however, that crackles of similar amplitude may correspond to either a relatively large or a much smaller $\dot{V}$ transient. Through determination

of the LF (<60 Hz) and HF (>1 kHz) components of each crackle, it could be demonstrated that crackles with significant LF energy were always associated with detectable transients in $\dot{V}$, whereas those that had low LF energy were not. Another interesting feature of these data was that, after a $\dot{V}$ transient marked by crackles with significant LF energy, the mean level of $\dot{V}$ was usually elevated.

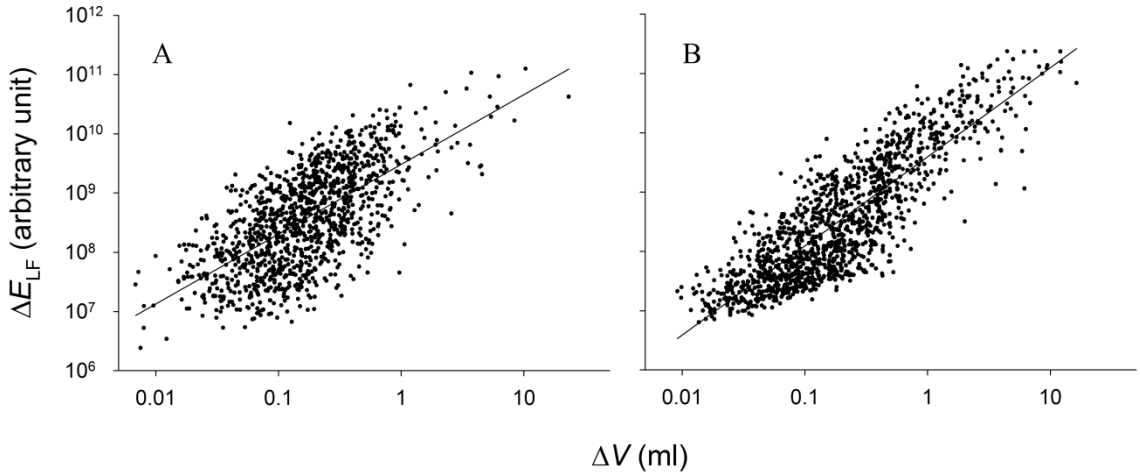

Fig. 11: Relationships between the values of discrete ΔV and the corresponding ΔE_{LF} pooled for all lobes for the first (A) and second (B) inflations.

To quantify the observed relationship between the LF energy of crackles and the recruited volumes associated with the $\dot{V}$ transients, the corresponding pairs of ΔE_{LF} and ΔV pooled for all lobes were plotted. Linear regressions were carried out in the log-log domain ($\log\Delta E_{LF} = \delta \cdot \Delta\log\Delta V + C$), and according to the unpaired *t*-test on these data, the slopes δ of the regression lines were significantly larger than unity for both the first ($p<0.002$) and the second ($p<0.001$) inflation. Additionally, the slope corresponding to the second inflation (δ =1.50±0.03) was significantly larger ($p<0.001$) than that corresponding to the first inflation (δ =1.18±0.04). The relationship $\Delta E_{LF} = C \cdot \Delta V^{\delta}$ was stronger for the second (r^2 = 0.73) than for the first inflation (r^2 = 0.44). In the individual lobes too, the second inflations always resulted in higher correlation coefficients (r^2 = 0.68 - 0.82) than those for the first manoeuvres (r^2 = 0.29 - 0.73).

To characterize the irregularities in ΔV and to calculate their probability density distribution, all data were combined (Fig. 12). The distribution probability of ΔV peaked between 0.02 and 0.05 ml and then decreased linear by in the log-log graph, indicating that the tail of the distribution follows a power law, *i.e.* $p(\Delta V) \sim \Delta V^{-\gamma}$. The exponents γ were 2.02±0.09 and 1.88±0.14 for the first and the second inflations, respectively. The exponent γ during the

first inflation was not significantly different from 2. However, even though γ from the second inflation was only 6% smaller than the theoretically expected value of 2, or 7% smaller than the value of 2.02 from the first inflation, this difference was statistically significant (p<0.03).

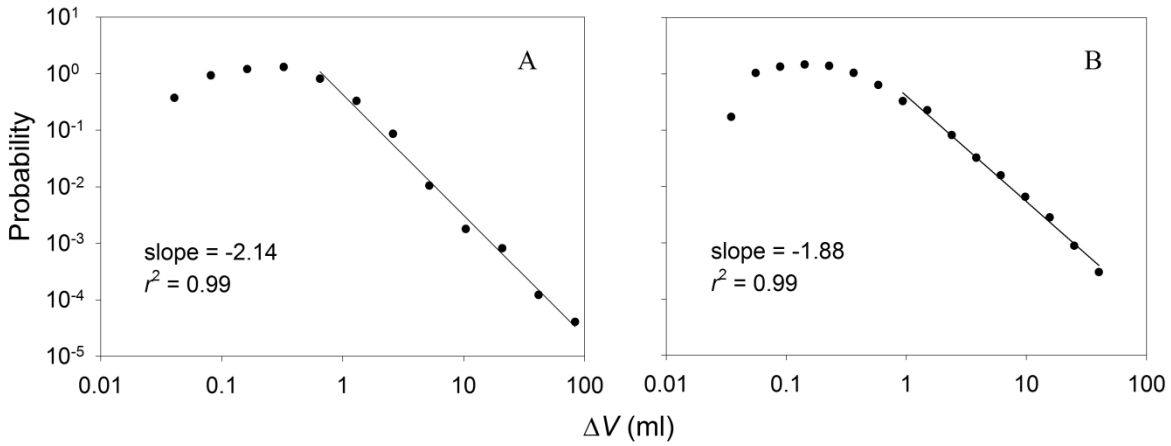

Fig. 12: Log-log plots of the probability distributions of discrete ΔV pooled from all first (A) and second (B) inflations. The lengths of the regression lines (solid lines) correspond to the ranges included in the regressions.

4.2. Crackle recording to monitor recruitment in bronchoconstriction (Study 2)

An example of the inflation P_L–V curves and the distributions of N_C, obtained under the control conditions and after the two highest doses of Mch at both P_L levels, is presented in Fig. 13. At a P_L of 4 hPa, the bottom knee in the P_L–V diagram was not apparent until the highest doses of Mch, whereas it was typically observed even under the control conditions at 1 hPa. It is worth noting that, in general, the crackle intensity increased significantly before the P_L–V curve displayed any alteration indicative of the development of the bottom knee (Fig. 13c). The histograms of the crackles exhibited their maxima at or slightly above the bottom knee and decayed rapidly around the highest slope of the P_L–V curve. The crackles disappeared before the upper knee was reached in the P_L–V diagram.

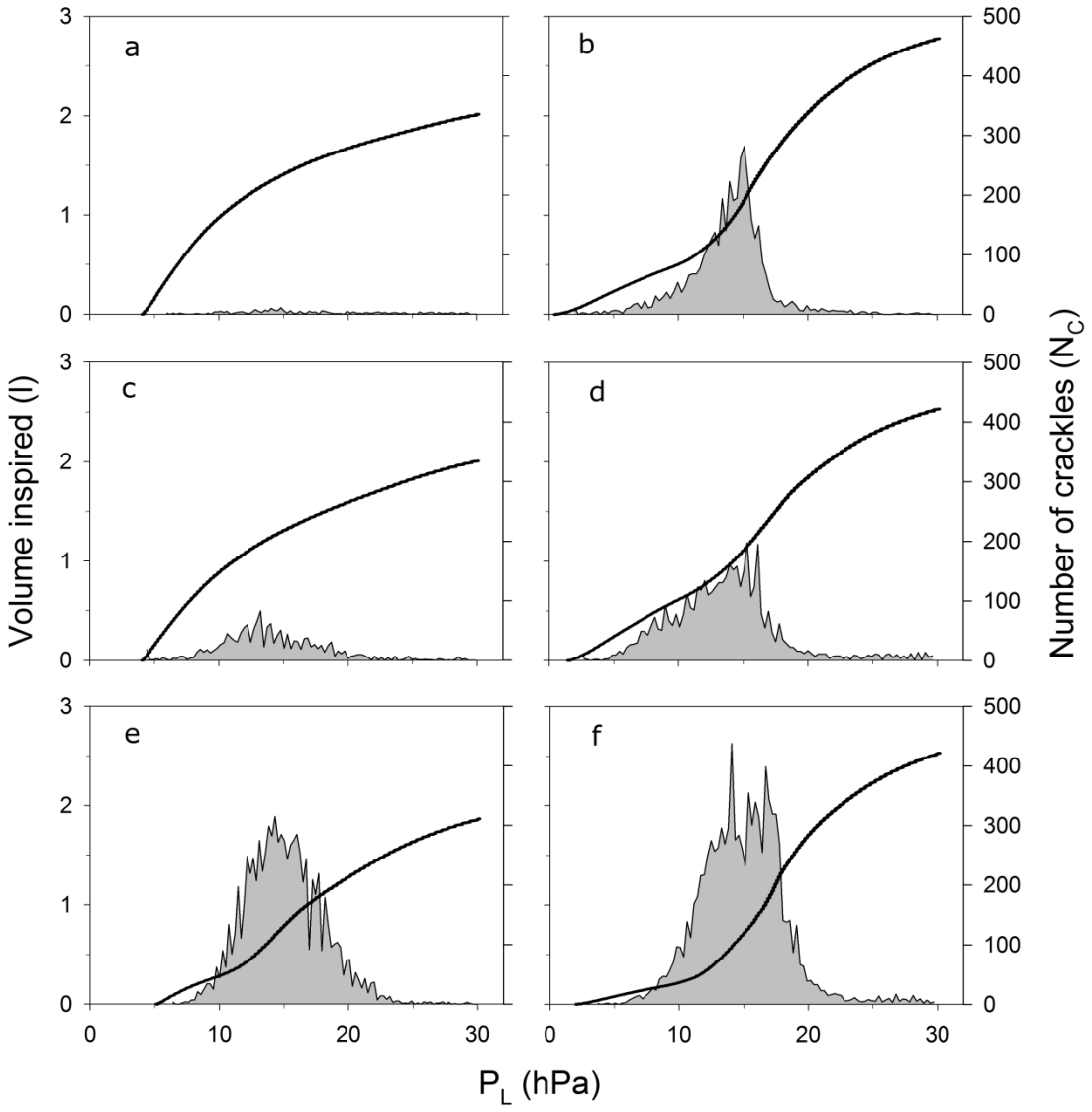

Fig. 13: Inspired V and N_C *vs* P_L from a typical experiment. Panels a, c and e show inflations from a P_L of 4 hPa under the control conditions and after 20 and 40 mg·kg^{-1} of Mch, respectively. Panels b, d and f relate to the corresponding inflations from a P_L of 1 hPa in the same animal.

Increasing doses of Mch induced progressive increases in N_C (Table 1), with statistically significant elevations from the control values first being observed at the dose of 20 μg·kg^{-1} at the PEEP of 4 hPa; overall, an average 38-fold rise occurred in N_C between the control level and the highest Mch dose. Statistical significance was reached already at the lowest dose at 1 hPa, where the crackle activity was already considerable (>1,000) under the control conditions, whereas at the highest 3 doses the PEEP dependence of the crackle number disappeared.

Table 1. Mean±SD values of N_C at two PEEP levels and different Mch doses.

	control	Mch 5 µg·kg^{-1}	Mch 10 µg·kg^{-1}	Mch 20 µg·kg^{-1}	Mch 40 µg·kg^{-1}
PEEP=1 hPa	1,494±1,383$^{\#}$	1,517±1,385$^{*\#}$	1,936±1,810*	3,464±3,972*	3,539±1,575*
PEEP=4 hPa	87±67	331±320	636±712	2,062±3,186*	3270±3,137*

*Significantly different (p<0.05) from the corresponding control data; $^{\#}$significantly different from the data at PEEP=4 hPa.

4.3. Crackles and airway function in emphysematous mice (Study 3)

PPE treatment resulted in statistically highly significant changes in V_Ls. The FRC and TGV20 (the TGV at a P_{rs} of 20 hPa) increased by 52 and 45% in group C1 and group E1, respectively, relative to the control. The average TGV *vs* P_{rs} curves also reflected significantly different values (p<0.001) between the groups at all P_{rs} levels. The ratios of the TGV between the groups at the same P_{rs} were fairly constant, suggesting a nearly proportional increase in TGV at all P_{rs} values, *i.e.*, an unchanged shape of the P–V loops. The inspiratory volume (TGV20 - FRC) increased by 37% in the treated animals.

The changes in the mechanical parameters were most marked in H, which decreased by 57 and 27% at P_{rs} values of 0 and 20 hPa, respectively. Small, but statistically insignificant decreases were observed in R_{aw} at both 0 hPa (-2%) and 20 hPa (-10%).

The vital capacity (VC) manoeuvres performed in the group C2 and group E2 animals also revealed marked differences in all V_Ls but the RV; a typical example is shown in Fig. 14A. Interestingly, the P at the bottom knee in the TGV–P_{rs} curve decreased on average by 5.5 hPa in the treated animals.

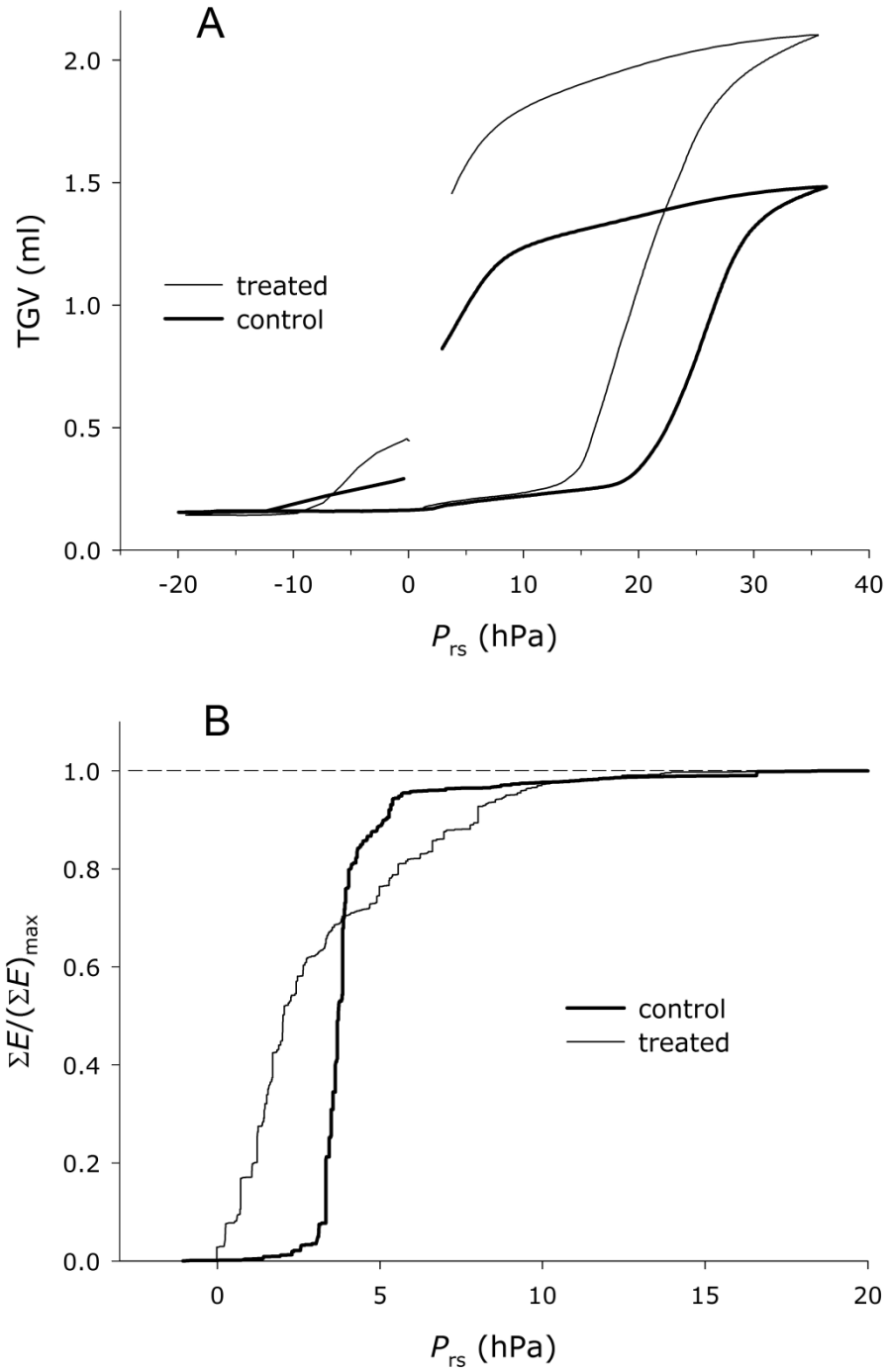

Fig. 14: A: Thoracic gas volume (TGV) *vs* transrespiratory pressure (P_{rs}) curves recorded during VC manoeuvres in a control (group C2) and a PPE-treated (group E2) mouse. Arrows indicate the bottom knees in the inflation curve. B: Cumulated crackle sound energy ΣE normalized by its maximum value $(\Sigma E)_{max}$ in the control and the treated mice. The data in both groups are pooled.

N_C detected during inflation from the RV to the TLC was ~150 and did not differ between the group C2 and group E2 mice. The cumulative distributions of crackle energy in groups C2 and E2 are compared as functions of P_{rs} in Fig. 14B. In group C2, the cumulative energy rose steeply from 0 to above 95% within a narrow range of P_{rs} values between 2.5 and

~5 hPa. In contrast, the cumulative energy in the group E2 rose almost immediately at the start of inflation, but reached 95% only by a P_{rs} of ~9 hPa. Despite the grossly different rates of crackle energy release during inflation, the probability distributions (Π) of the crackle amplitudes in the two groups were very similar (Fig. 15).

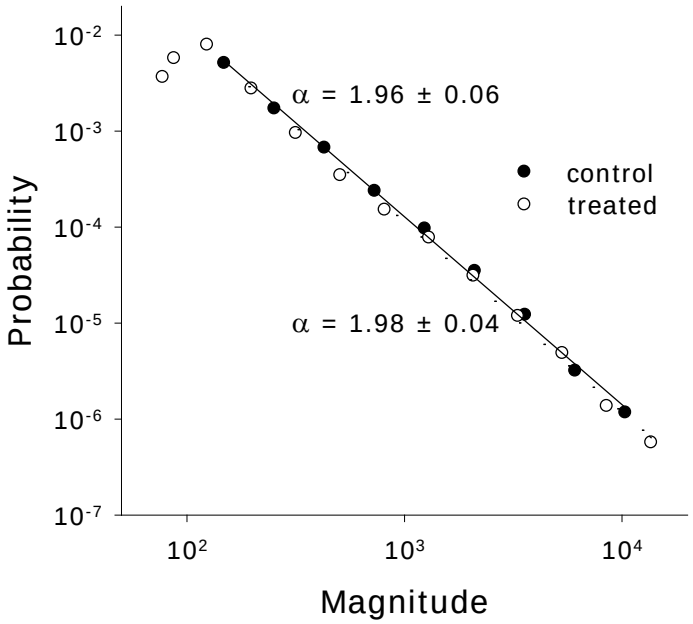

Fig. 15: Log-log plots of the probability distributions of the crackle amplitude (in arbitrary units) recorded during inflations from the RV to the TLC in the control (group C2) and the PPE-treated (group E2) mice. Pooled data are from 3 to 5 inflation manoeuvres in each mouse. The regression lines cover the data range included in the regression.

Since both distributions decreased linearly in a log-log graph, Π can be described by a power law as $\Pi \sim s^{-\alpha}$, where s is the crackle amplitude and α is the exponent of the distribution. Furthermore, α exhibited identical values (close to 2 with a small standard deviation) in the two groups of mice.

4.4. Crackles and airway structure/function in emphysematous rats (Study 4)

The FRC and RV were statistically significantly higher in the PPE group as compared with the controls (by 38% and 53%, respectively); however, the increase in TLC in the treated rats was not significant.

Whereas the tissue mechanical parameters G and H were statistically significantly smaller (76% and 62%) in the PPE-treated rats than in the controls, there was no difference in

R_{aw} between the groups. Because of the larger differences in H, tissue hysteresivity ($\eta = G/H$) was elevated (129%) in the treated rats.

The lower knee in the inflation P–V curves from the degassed state (as defined by the intercept of the lines fitted to the P–V curve between 5 and 15, and the maximum slope projected to the P axis) was shifted to higher Ps (19.3±1.0 *vs* 17.8±1.2 hPa; p=0.021) and the asymptotic volume level (TLC) was slightly larger in the PPE group than in the control rats (Fig. 16).

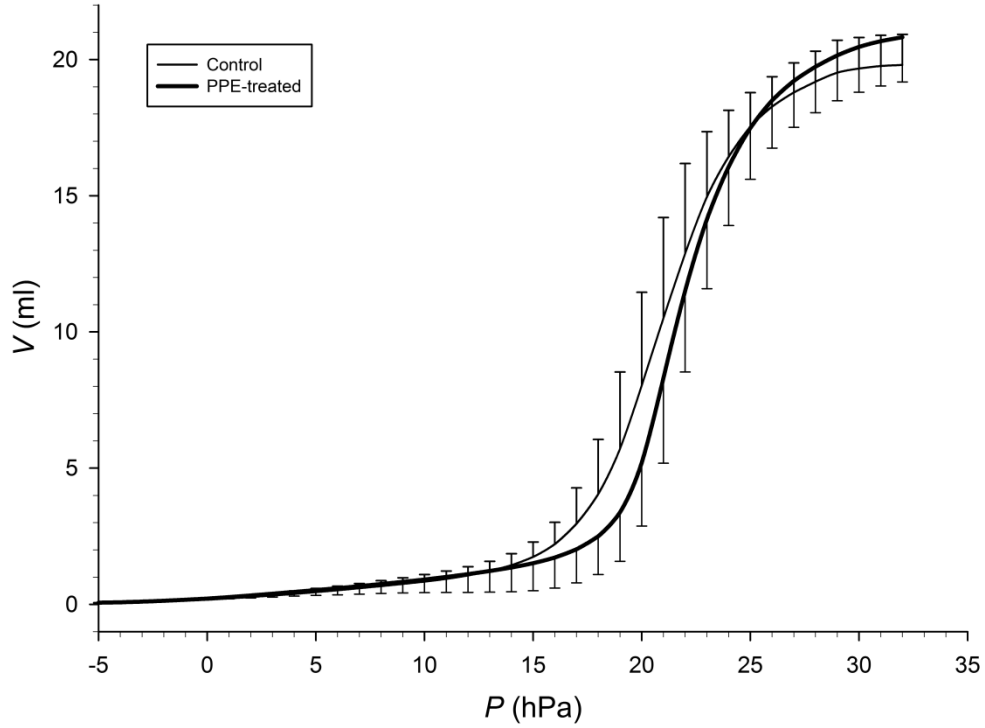

Fig. 16: Comparison of the inflation P–V curves of the control (thin line) and PPE (thick line) groups from the degassed state (mean±SD).

The number of bronchial cross-sections analysed in each rat ranged between 40 and 50. According to the bronchial morphometry, there was no difference between the D_b of the airways of the control and the PPE-treated animals. The attachment density N_s/P_b was mildly, but statistically significantly lower in the PPE group (median 0.0175 *vs* 0.0189 μm^{-1}; p<0.001). Regression analysis showed that T_w did not depend on D_b in either group. However, the mean value of T_w was higher in the PPE group than for the controls (12.4 *vs* 10.8 μm; p<0.0001). The average, the spatial variability of the elastin density and the total elastin content within the bronchial wall did not differ between the groups. The collagen density and its intra-bronchial SD were increased by 12% and 17% in the treated group (p<0.05).

Furthermore, the inter-airway variance of the collagen density was substantially higher (67%, $p<0.01$) in the treated animals. The densities of elastin and collagen did not correlate with D_b.

The N_C per inflation were not different between the two groups (1,152±593 *vs* 1,203±538; $p=0.778$); however, their distributions expressed as relative frequencies (N_C/N_{total}) were statistically significantly different ($p<0.001$). In the control rats, N_C peaked at lower *P*s (~10 hPa) than it did in the PPE group (~17 hPa), and exhibited another maximum at ~25-30 hPa (Fig. 17a). This latter fact suggests a bimodal distribution of the sounds of reopening, which is also expressed by the $\log(N_C/N_{total})$ *vs V* graphs exhibiting a second peak at ~19-23 ml in the control group (Fig. 17b).

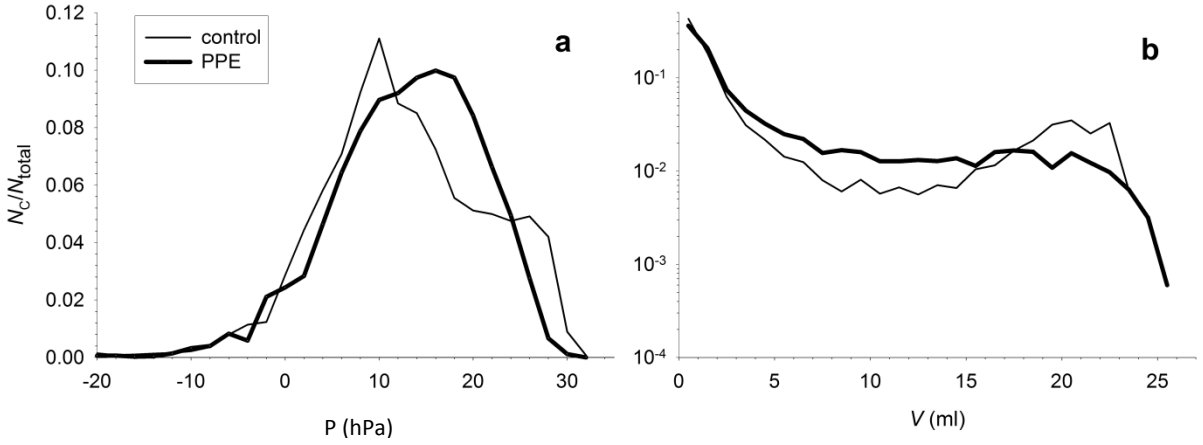

Fig. 17: Relative frequencies (N_C/N_{total}) of crackles in the control and PPE groups as a function of *P* on a lin-lin scale (a) and *V* on a lin-log scale (b).

5. Discussion

5.1. Acoustic evidence of airway opening during recruitment (Study 1)

In this study, we investigated the possibility that the process of airway opening contributes to alveolar recruitment and the lower knee in the *P–V* curve of the lung. We employed an experimental setup in which the *P–V* curve and crackles, as indicators of airway opening, were simultaneously recorded in isolated dog lung lobes. The main findings were that *1*) recruitments occurred in discrete Δ*V*s; *2*) the discrete Δ*V*s were accompanied by crackles carrying LF energy; *3*) in the presence of trapped air, the inflation exhibited a biphasic behaviour resulting in two distinguishable lower knees in the *P–V* curve; and *4*) the distribution of Δ*V* followed a power law.

A characteristic feature of the results was that, for both the first and second inflations, the vast majority of the crackles occurred before $\dot{V}$ reached its maximum value (Fig. 8). Since crackles are successively attenuated at every bifurcation as they propagate from the site of generation towards the trachea [5], this pattern suggests that the opening phenomena progressed from the central to the peripheral airways. The attenuation factor can be calculated from the ratio of cross-sectional areas at bifurcations, and it has been reported to be ~0.65 for the airway tree of the dog [5]. As every bifurcation attenuates the crackle amplitude by 0.65 on average, crackles that were generated deeper in the lung became significantly attenuated once they passed >10 bifurcations. Indeed, as shown in Fig. 9, the sound energy decreased by several orders of magnitude when the inflation reached the lower knee in the *P–V* curve, and this is consistent with the decreasing envelope of the crackle time series.

During the second inflation, the cumulative sound energy reached its 95% level at a lower inflation *P* as compared with the first inflation, which was accompanied by a biphasic shape of the $\dot{V}$ *vs* time curve (Fig. 8) and two separate lower knees in the *P–V* curve (Fig. 9). We explain the biphasic process in the second inflations as follows. Since the lobes were not degassed after the first inflation, increased air trapping occurred, as indicated by an apparently greater lobe size before the second inflation was started. The airways leading to the trapped air regions opened first in the inflation process, and this resulted in transients in $\dot{V}$ greater than those observed in the first inflation; in view of the fact that the subtended clusters of open alveoli were ready to accommodate a higher $\dot{V}$ at the moment of the airway opening, the elevation in *V* can be sudden (Fig. 9) and associated with a halt in the *P* increase, even leading

to an unstable *P*–*V* relationship [64]. Subsequently, the reopened trapped regions became distended, causing a fall in the central $\dot{V}$, due to the rest of the collapsed lobe still being in an early phase of recruitment. As the open regions continued to inflate, *P* increased further, which in turn resulted in a gradual opening of the remaining collapsed regions. The biphasic pattern of reopening was characteristic of any subsequent inflations occasionally performed (results not shown). Although such a behaviour may also occur during the inflation of *in vivo* lungs under conditions where regions of trapped air and atelectasis coexist, caution is demanded in the extrapolation of these results to the inflation of the ARDS lung, where the situation is further complicated by a surfactant dysfunction and/or flooding of the alveoli [26].

Crackles can be regarded as direct signatures of individual airway openings, which can be considered "microscopic" events contributing to the "macroscopic" *P*–*V* curve of the lung [32]. The mechanism by which a crackle sound is generated is not well understood, but several concepts have been proposed [8, 24, 32]. We believe that the mechanism that is most likely in the excised lungs that we studied is that crackles are a consequence of the rapid break-up of the fluid meniscus inside a closed airway, with a small amount of air behind the closure [32]. In terms of temporal properties, we argue that crackles of short duration, consisting of the initial sharp sound of the break-up of the fluid meniscus alone, may mark the opening of a single airway segment without a noticeable increase in lung *V*, whereas crackles that also include an elongated ringing with a significant LF energy mark the entry of $\dot{V}$ into a larger peripheral region. This latter crackle type indicates the sudden recruitment of lung *V*, which we have termed a discrete ΔV, to distinguish it from the continuous *V* change corresponding to the elastic expansion of the recruited airspaces. Intuitively, for the whole lung, the sequence of opening events (at least those that trigger a change in mean $\dot{V}$ as illustrated by the type *c* openings in Fig. 10) can be associated with the discrete incremental component of the *P*–*V* curve as opposed to the continuous component reflecting the elastic expansion of the lung. If all $\dot{V}$ transients could be detected and the corresponding discrete *V* increments ΔV cumulated, we would be able to reconstruct that part of the *P*–*V* curve that is formed by the discrete *V* recruitments. There are fundamental limitations in the detection of each ΔV, however, imposed by both the sensitivity and the temporal resolution of the measurement of $\dot{V}$, especially in the middle part of the inflation, where the densely overlapping $\dot{V}$ transients cannot be separated. The number of ΔVs estimated by the manual determination of the time limits of the transients of $\dot{V}$ ranged from 54 to 310 in an inflation, which contrasts with the much larger N_C (ranging from 3,800 to 14,800), which were

identified automatically by exploiting the finer temporal resolution and the higher signal-to-noise level in the high-pass-filtered sound recordings.

The distribution of the recruited ΔVs has been predicted to be a power law with an exponent of 2 [21] and has recently been measured indirectly [6]. Our data reflect a direct assessment of the distribution of alveolar recruited ΔVs. During both the first and second inflations, the distribution displays a plateau-like region for small ΔV, followed by a region of about two decades over which the distribution decreases linearly in the log-log graph, *i.e.* it follows a power law form. The plateau region is obviously due to the limitation of the measurement: even though the flow meter is able to measure very small $\dot{V}$s corresponding to ΔVs of 0.1 ml, below this limit the data are not reliable. It is also possible that two or more small ΔVs occur simultaneously which results in a lower number of small ΔV values. Nevertheless, for the first inflation, the data were in excellent agreement with the model prediction [21] since the theoretical value of the exponent is 2, whereas the estimated average one was 2.02. The distribution obtained from the second inflation had an exponent of 1.88, which is also close to the theoretical value of 2. The reason for this small discrepancy is unclear, but it may be due to the fact that the presence of significant trapped air terminates the avalanches in larger alveolar regions than in the fully collapsed lung. As a consequence, slightly more larger ΔV values would be recorded than during the first inflation, which in turn leads to a longer tail of the distribution. Nevertheless, the power law distribution implies that, even in the presence of trapped air, each phase of the biphasic recruitment process corresponding to the two lower knees in the P–V curve is likely to involve predominantly avalanche-like airway openings.

5.2. Crackle recording to monitor recruitment in bronchoconstriction (Study 2)

In order to characterize the recruitment processes during an acute pulmonary constriction in mechanically ventilated animals, intratracheal recordings of crackles during slow inflations were made in open-chest pigs. Airway closure was generated by lowering the lung V and/or inducing lung constriction with Mch.

The results of the experiments revealed that: 1) the development of the lower knee in the P_L–V curve was always associated with a significant increase in crackle activity; 2) the N_C increased with the dose of Mch administered before the reinflation from the PEEP level and 3) while the PEEP level (1 *vs* 4 hPa) was an important determinant of the crackle activity in

the control group and at low doses of Mch, at high Mch doses the bronchoactive factor predominated.

In order to quantify the reopening of lung units during obstructive disorders in mechanically ventilated mini-pigs, a crackle measurement technique was adopted that was previously employed in excised dog lungs (Study 1, [1]). Although it has been proposed that crackles are generated by the abrupt reopening of lung units [8, 14, 65], evidence has been presented only recently that lung crackles originate from the sudden reopening of the conducting airways (Study 1, [1, 16]). Since the acoustic events identified in these *in vivo* pig experiments were very similar to those described previously (Study 1, [1, 16]), it is assumed that they also originate from the opening of small lung structures.

The fact that N_C plateaued with increasing doses of Mch may reflect the limit set by the noise to the sensitivity of crackle detection, and explain why the progression of reopenings towards the periphery could be followed until N_C reached a value of ~4,000 (corresponding to the 11th airway generation). Although the acoustic tracking of the recruitment process may have been incomplete, it is important to note that, to the best of our knowledge, this is the first *in vivo* study in which the development of the full inspiratory *P*–*V* curve was accompanied by the recording of reopening sounds. Whilst the crackles were hardly recognizable (either acoustically or visually) in the original sound recordings because of the strong cardiogenic sounds, simple but appropriate high-pass filtering revealed the abundant crackles accompanying the reopening process. On the other hand, elimination of the LF content of the crackles precluded the possibility of assessing the *V* increments on the basis of the crackle after-rings; likewise, the cardiogenic component of $\dot{V}$ completely masked the ΔVs associated with the reopenings.

The use of an open-chest preparation made it possible to lower the lung *V* below the closing *V*, thereby facilitating closure of the airways even without a bronchoconstrictor challenge. Indeed, re-inflation from a P_L of 1 hPa under control conditions resulted in a reopening activity comparable in N_C to that reached at the third dose of Mch at the higher P_L level.

The aim of this study was to quantify the lung recruitment via the crackle activity recorded during the subsequent slow inflations at different mean lung *V*s and degrees of bronchoconstriction. The experimental model was therefore chosen to mimic situations characterized by airway obstruction, such as in anaphylactic reactions, the exacerbation of asthma or COPD, and was not intended to include capillary filtration/resorption abnormalities

typical of an acute lung injury. Excessive intrabronchial fluid and foam production in pulmonary oedema may increase the number of crackle-like sounds not uniquely connected to airway opening; bubbles may pop up in large numbers during both inspiration and expiration, and produce transient sounds reminiscent of crackles [5]. This did not happen in the present study; gross examination of the lungs and major airways revealed no fluid accumulation, and the lung mechanics had almost completely recovered by the beginning of the second sequence of Mch challenges [2].

5.3. Crackles and airway function in emphysematous mice (Study 3)

The primary purpose of this study was to characterize the behaviour of the airways during slow inspiratory VC manoeuvres in a mouse model of emphysema. To achieve this goal, we used a standard PPE treatment protocol and confirmed the presence of emphysema in the treated mice 3 weeks following the treatment on the basis of lung *V*s and respiratory mechanics.

The main findings of the study are as follows. (1) We observed increases in TGV similar to those seen in FRC and TLC in patients with emphysema; (2) the dynamic elastance was significantly lower in the treated mice, whereas the airway resistance was not different. Measurements made in two additional groups of mice revealed that (3) the PPE treatment did not lead to any increase in RV, whereas the bottom knee in the *P*–*V* curve was shifted to lower P_{rs}, and (4) although the cumulated crackle energy increased more slowly during inflation in the treated mice, the probability distributions of crackle amplitudes were very similar.

Since the RV is most sensitive to small airway collapse, the little or no change in RV implies that the small airways, whose closure determines the RV, were not influenced by PPE treatment. Interestingly, the lower knee in the *P*–*V* curve (Fig. 14A) shifted to a lower P_{rs}, and the cumulative crackle energy started to increase at a much lower P_{rs} in the treated mice (Fig. 14B). Both of these findings suggest that a significant fraction of the airways had a lower critical opening P_{rs} in the treated animals. How is it possible then that, whereas the RV and R_{aw} at the same P_{rs} are the same in the control and treated mice, the lower knee and the crackle energies are different in the two groups?

The lower knee in the inflation curve is associated with massive airway opening, leading to alveolar recruitment [30], although the crackles that were detectable in our experiments may have come from larger airways than those that determine the RV. Thus,

although the site of airway closure and the trapped air behind the small airways that determine the RV are similar in the two groups, the relative locations of the knee in Fig. 14A imply that some of these airways are easier to open in the emphysematous group. In contrast, since a weakened parenchymal tethering, which characterizes group E2, reduces the probability of airways reopening, one might expect that the opening P_{rs} would actually be higher in group E2. In fact, on examination of the cumulative distributions in Fig. 14B, both of these statements are seen to be true. Indeed, the difference in cumulative crackle energy suggests that some airways must be more difficult to open in group E2 since 95% of the total energy is reached only at P_{rs} of 9 hPa, as compared with a P_{rs} of ∼5 hPa in group C2. On the other hand, there are crackles that are triggered at a much lower P_{rs} in group E2 than in group C2, indicating that some airways in the former group open very easily. Although the reduced tethering in group E2 explains why some airways are more difficult to open in group E2, we are unsure about the exact mechanism responsible for the reduction in the airway opening P_{rs} following treatment. Assuming that the surface tension is not altered by the PPE treatment, we can speculate as follows. Computer simulations mimicking the breakdown of the lung parenchyma have shown that, when the breakdown is governed by mechanical forces, a significant heterogeneity develops in the network [66]. This leads to a broad distribution of mechanical forces around the damaged area, including elastic elements that carry both significantly smaller and larger forces than before the breakdown [67]. The higher forces would then generate increased tethering locally and hence a reduced opening P_{rs}.

The above uncertainties indicate that further investigations involving time course studies with a longer time period after PPE treatment are warranted to shed further light on the relevance of this murine model of emphysema to the human disease.

5.4. Crackles and airway structure/function in emphysematous rats (Study 4)

In this rat model of emphysema, we investigated the alveolar and bronchial structural changes underlying the alterations in lung V and mechanics, and the acoustic manifestations of the airway function. The combination of structural and functional measurements revealed that (1) the PPE treatment caused significant increases in the FRC and the RV, but only a small change in the TLC; (2) the tissue mechanical parameters were significantly lower in the treated group, whereas there was no detectable alteration in the total airway resistance as measured at the FRC; (3) the alveolar attachment density was lower and T_w was higher in the emphysematous animals; (4) while no difference was found in the elastin content per unit T_w

of the bronchial wall, the collagen content was higher and more heterogeneous in the treated animals; (5) while the N_C per inflation was similar, the distributions of crackles as a function of P_{rs} or lung V were statistically significantly different in the PPE-treated and control groups, and (6) the lower knee in the inflation $P–V$ curve was shifted to higher P_{rs} in the treated rats.

We attribute the increase in opening P_{rs} in the emphysema group to the decrease in parenchymal tethering forces transmitted to the walls of the sequentially opening segments of the airway tree. This shift in the inflation $P–V$ curve was consistent with a delayed recruitment process, also indicated by the crackle intensity.

R_{aw} was not different in the two groups, which suggests that the overall resistance of the bronchial tree was not affected by the PPE treatment. This is in accord with our findings in mice (Study 3, [3]). The knee in the $P–V$ curve was shifted statistically significantly to higher P_{rs} in the treated rats, which was in contrast with the observations in mice (Study 3, [3]). Since the lower knee in the $P–V$ curve signifies airway openings [30], this shift implies that the critical opening P_{rs} at which massive airway opening allows the alveoli to start filling up was higher in the treated lungs. The reasons for this discrepancy between the mice and rats (investigated with very similar protocols) are not clear; perhaps, the difference in the elastic properties of the chest wall transmitting the P_{rs} to the lung surface (a lower murine chest elastance with a faster transmission) is one possible explanation.

In the present study, we quantified the strength of parenchymal tethering by measuring the number of attachments per unit airway wall perimeter and found that the treatment reduced the average attachment density by 7%. There was no difference in airway diameter between the control and treated groups at the same lung fixation P, which suggests that the reduction in attachment density was probably due to loss of parenchymal walls around airways.

The elastin density of the walls was similar in the two groups. Since T_w was larger in the treated animals, it is likely that the total elastin content was also larger in the bronchial walls of the treated rats, implying cellular remodelling of the airway walls. However, collagen also contributes to stiffness, especially at higher P_L, and the increased collagen density of the wall with the elevated intra-wall heterogeneity suggests a disordered cellular remodelling following PPE treatment.

The results from the crackle sounds also revealed major differences in the distribution of N_C as a function of airway P or lung V (Fig. 17). The amplitude distribution of the crackle

sounds followed a power law, in agreement with previous studies in normal dog lungs [5] and in PPE-treated mice (Study 3, [3]).

The exponent α of the power law distribution has been shown to reflect the average bifurcation geometry of the airway tree [5]. Specifically, $\alpha=ln(2/b)/ln(b)$, where $b=2A_1/(A_0+A_1+A_2)$ and A_0 is the cross-sectional area of the parent airway, A_1 is the cross-sectional area of the daughter branch from which the crackles come, and A_2 is the cross-sectional area of the other daughter branch. Assuming that, on average, the bifurcation geometry is symmetric (*i.e.* $A_1=A_2$) and knowing α and hence b from experiments, we can estimate the average diameter ratio d_1/d_0 at the bifurcations. The values of b in the control and treated rats were 0.573 and 0.512, respectively, yielding in corresponding diameter ratios of 0.757 and 0.712. The assumption of symmetric bifurcations seems unwarranted, and it is possible to show on the basis of earlier work [5] that similar results can be derived by using asymmetric bifurcations (unpublished data). This analysis suggests then that, on average, the airway diameters decrease faster along the airway tree in the treated animals than in the control animals, which seems to contradict the fact that R_{aw} did not differ between the two groups. However, whereas R_{aw} characterizes air flow resistance around FRC, the distribution of crackle amplitudes mostly reflects diameters at much higher lung Vs than FRC. Furthermore, the reduced diameter ratio obtained from crackles is also in accord with both a stiffer wall due to increased collagen content and T_w, and a reduced parenchymal tethering as a result of the lower attachment density and septal stiffness. We therefore conclude that the reduced diameter ratio inferred from the crackles and the shift in the knee in the P–V curve imply an important deterioration in airway patency under conditions such as airway reopening and high lung V that the FOT-based R_{aw} measured around the FRC does not detect.

Summary and conclusions

1. We have observed that in the reinflation of isolated collapsed lungs the elastic expansion of the alveoli is intermittently interrupted by discrete volume increments, which are accompanied by acoustic events. The majority of crackles were detected near the lower knee in the inspiratory pressure–volume curve. Hence, in contrast with the prevailing view that recruitment occurs at the alveolar level, our data provide strong evidence that the recruitment of alveolar regions is a highly irregular process triggered by avalanche-like airway openings. We also found that the lower knee in the pressure–volume curve shifts to lower pressures, in the presence of trapped air, but the knee is still dominated by airway openings. Thus, airway opening is an important determinant of the recruitment process of the partially collapsed and also fluid-filled lung in ARDS.

2. We have demonstrated that the quantification of airway closure on the basis of subsequent recruitment is feasible by recording and processing intratracheal crackle sounds *in vivo*. The measurements revealed the importance of airway closure and reopening in the development of the pressure–volume characteristics following the administration of methacholine at a normal lung volume, and especially at a lung volume below the closing volume. Lung sound recording appears to be a sensitive tool with which to indicate early impairments in the mechanics of the lung periphery. Thus, crackle recordings may have the potential to serve as a bedside monitoring tool for detection of the cyclic recruitment-derecruitment of the airways during mechanical ventilation, and hence contribute to the guidance of the optimum ventilation strategy.

3. We have investigated the effects of elastase treatment on the airway function in established rodent models of human emphysema exhibiting enlarged airspaces, in order to ascertain whether or not the treatment also leads to enhanced collapsibility and hindered reopening of the airways, as a result of weakened parenchymal tethering. While the treatment resulted in marked changes in lung volumes, the airway resistance measured at the level of the FRC did not change either in mice or in rats. There was no alteration in the size distribution of crackles between the control and treated animals; however, subtle changes in recruitment dynamics and airway morphometry were observed. We conclude

that the reduced parenchymal tethering and an increased stiffness of the remodelled bronchial wall acted oppositely, and these rodent models therefore need to be refined and followed on a longer time scale in order to mimic the human disease to a better extent.

Acknowledgements

First and foremost, I wish to express my grateful thanks and appreciation to my supervisor, Professor Zoltán Hantos, for his invaluable help towards the preparation of my thesis. I greatly appreciate his excellent and indispensable guidance in the experimental work, data analysis and interpretation.

I also wish to thank Professor Béla Suki for his continuous active support, his highly effective tutoring and the stimulating discussions, which have helped me so much throughout the years of my research.

I would also like to thank Dr. Ágnes Adamicza and Dr. Margit Szabari for the possibility to work with them in the laboratory and for their introducing me to the basic skills of animal experimentation.

I further express my deep gratitude to all the co-workers and the laboratory staff who have supported my research at the Department of Medical Physics and Informatics, the Institute for Surgical Research, University of Szeged, and the Department of Biomedical Engineering, Boston University.

***

The work presented in this thesis was supported by Hungarian Scientific Research Fund grants OTKA T30670, F038340, T37810, T42971 and 67700, National Science Foundation grants BES-0114538, BES-0402530, National Institutes of Health grant HL090757 and Swiss National Science Foundation grant 3200-064899.01/1.

References

1. Hantos, Z., J. Tolnai, T. Asztalos, F. Petak, A. Adamicza, A.M. Alencar, A. Majumdar, and B. Suki, *Acoustic evidence of airway opening during recruitment in excised dog lungs.* Journal of Applied Physiology, 2004. 97(2): p. 592-8.
2. Petak, F., W. Habre, B. Babik, J. Tolnai, and Z. Hantos, *Crackle-sound recording to monitor airway closure and recruitment in ventilated pigs.* Eur Respir J, 2006. 27(4): p. 808-16.
3. Hantos, Z., A. Adamicza, T.Z. Janosi, M.V. Szabari, J. Tolnai, and B. Suki, *Lung volumes and respiratory mechanics in elastase-induced emphysema in mice.* Journal of Applied Physiology, 2008. 105(6): p. 1864-72.
4. Tolnai, J., M.V. Szabari, G. Albu, B.A. Maar, H. Parameswaran, E. Bartolak-Suki, B. Suki, and Z. Hantos, *Functional and morphological assessment of early impairment of airway function in a rat model of emphysema.* Journal of Applied Physiology, 2012. [Epub ahead of print] PMID: 22442024.
5. Alencar, A.M., Z. Hantos, F. Petak, J. Tolnai, T. Asztalos, S. Zapperi, J.S. Andrade, Jr., S.V. Buldyrev, H.E. Stanley, and B. Suki, *Scaling behavior in crackle sound during lung inflation.* Phys Rev E Stat Phys Plasmas Fluids Relat Interdiscip Topics, 1999. 60(4 Pt B): p. 4659-63.
6. Suki, B., A.M. Alencar, J. Tolnai, T. Asztalos, F. Petak, M.K. Sujeer, K. Patel, J. Patel, H.E. Stanley, and Z. Hantos, *Size distribution of recruited alveolar volumes in airway reopening.* Journal of Applied Physiology, 2000. 89(5): p. 2030-40.
7. Majumdar, A., Z. Hantos, J. Tolnai, H. Parameswaran, R. Tepper, and B. Suki, *Estimating the diameter of airways susceptible for collapse using crackle sound.* Journal of Applied Physiology, 2009. 107(5): p. 1504-12.
8. Forgacs, P., *Crackles and wheezes.* Lancet, 1967. 2(7508): p. 203-5.
9. Forgacs, P., *Functional Basis of Pulmonary Sounds.* Chest, 1978. 73(3): p. 399-405.
10. Forgacs, P., A.R. Nathoo, and H.D. Richardson, *Breath sounds.* Thorax, 1971. 26(3): p. 288-95.
11. Shinozuka, N., T. Nemoto, and J.H.T. Bates, *Isovolume bronchoconstriction by vagal stimulation in dogs: Effects of lung inflation pressure.* Respiration Physiology, 1998. 111(1): p. 79-88.
12. Piirila, P., A.R. Sovijarvi, T. Kaisla, H.M. Rajala, and T. Katila, *Crackles in patients with fibrosing alveolitis, bronchiectasis, COPD, and heart failure.* Chest, 1991. 99(5): p. 1076-83.
13. Piirila, P. and A.R.A. Sovijarvi, *Crackles: Recording, analysis and clinical significance.* European Respiratory Journal, 1995. 8(12): p. 2139-2148.

14. Nath, A.R. and L.H. Capel, *Inspiratory crackles and mechanical events of breathing.* Thorax, 1974. 29(6): p. 695-8.

15. Piirila, P., *Changes in crackle characteristics during the clinical course of pneumonia.* Chest, 1992. 102(1): p. 176-83.

16. Cheng, W., D.S. DeLong, G.N. Franz, E.L. Petsonk, and D.G. Frazer, *Discountinuous lung sounds and hysteresis in control and Tween 20-rinsed excised rat lungs.* Respir Physiol, 1999. 117(2-3): p. 131-40.

17. Amato, M.B., C.S. Barbas, D.M. Medeiros, R.B. Magaldi, G.P. Schettino, G. Lorenzi-Filho, R.A. Kairalla, D. Deheinzelin, C. Munoz, R. Oliveira, T.Y. Takagaki, and C.R. Carvalho, *Effect of a protective-ventilation strategy on mortality in the acute respiratory distress syndrome.* N Engl J Med, 1998. 338(6): p. 347-54.

18. Jonson, B., J.C. Richard, C. Straus, J. Mancebo, F. Lemaire, and L. Brochard, *Pressure-volume curves and compliance in acute lung injury: evidence of recruitment above the lower inflection point.* Am J Respir Crit Care Med, 1999. 159(4 Pt 1): p. 1172-8.

19. Lachmann, B., *Open up the lung and keep the lung open.* Intensive Care Med, 1992. 18(6): p. 319-21.

20. Muscedere, J.G., J.B. Mullen, K. Gan, and A.S. Slutsky, *Tidal ventilation at low airway pressures can augment lung injury.* Am J Respir Crit Care Med, 1994. 149(5): p. 1327-34.

21. Smaldone, G.C., W. Mitzner, and H. Itoh, *Role of alveolar recruitment in lung inflation: influence on pressure-volume hysteresis.* Journal of Applied Physiology, 1983. 55(4): p. 1321-32.

22. Crotti, S., D. Mascheroni, P. Caironi, P. Pelosi, G. Ronzoni, M. Mondino, J.J. Marini, and L. Gattinoni, *Recruitment and derecruitment during acute respiratory failure: a clinical study.* Am J Respir Crit Care Med, 2001. 164(1): p. 131-40.

23. Hickling, K.G., *The pressure-volume curve is greatly modified by recruitment. A mathematical model of ARDS lungs.* Am J Respir Crit Care Med, 1998. 158(1): p. 194-202.

24. Fredberg, J.J. and S.K. Holford, *Discrete lung sounds: crackles (rales) as stress-relaxation quadrupoles.* J Acoust Soc Am, 1983. 73(3): p. 1036-46.

25. Mergoni, M., A. Volpi, C. Bricchi, and A. Rossi, *Lower inflection point and recruitment with PEEP in ventilated patients with acute respiratory failure.* Journal of Applied Physiology, 2001. 91(1): p. 441-50.

26. Hubmayr, R.D., *Perspective on lung injury and recruitment: a skeptical look at the opening and collapse story.* Am J Respir Crit Care Med, 2002. 165(12): p. 1647-53.

27. Cheng, W., D.S. DeLong, G.N. Franz, E.L. Petsonk, and D.G. Frazer, *Contribution of opening and closing of lung units to lung hysteresis.* Respir Physiol, 1995. 102(2-3): p. 205-15.

28. Munakata, M., Y. Homma, M. Matsuzaki, H. Ogasawara, K. Tanimura, H. Kusaka, and Y. Kawakami, *Production mechanism of crackles in excised normal canine lungs.* Journal of Applied Physiology, 1986. 61(3): p. 1120-5.

29. Suki, B., A.L. Barabasi, Z. Hantos, F. Petak, and H.E. Stanley, *Avalanches and power-law behaviour in lung inflation.* Nature, 1994. 368(6472): p. 615-8.

30. Suki, B., J.S. Andrade, Jr., M.F. Coughlin, D. Stamenovic, H.E. Stanley, M. Sujeer, and S. Zapperi, *Mathematical modeling of the first inflation of degassed lungs.* Ann Biomed Eng, 1998. 26(4): p. 608-17.

31. Majumdar, A., A.M. Alencar, S.V. Buldyrev, Z. Hantos, H.E. Stanley, and B. Suki, *Characterization of the branching structure of the lung from "macroscopic" pressure-volume measurements.* Phys Rev Lett, 2001. 87(5): p. 058102.

32. Majumdar, A., A.M. Alencar, S.V. Buldyrev, Z. Hantos, H.E. Stanley, and B. Suki, *Fluid transport in branched structures with temporary closures: a model for quasistatic lung inflation.* Phys Rev E Stat Nonlin Soft Matter Phys, 2003. 67(3 Pt 1): p. 031912.

33. Sujeer, M.K., S.V. Buldyrev, S. Zapperi, J.S. Andrade, H.E. Stanley, and B. Suki, *Volume distributions of avalanches in lung inflation: A statistical mechanical approach.* Physical Review E, 1997. 56(3): p. 3385-3394.

34. Pasterkamp, H., S.S. Kraman, and G.R. Wodicka, *Respiratory sounds. Advances beyond the stethoscope.* Am J Respir Crit Care Med, 1997. 156(3 Pt 1): p. 974-87.

35. de Chazal, I. and R.D. Hubmayr, *Novel aspects of pulmonary mechanics in intensive care.* Br J Anaesth, 2003. 91(1): p. 81-91.

36. Dhand, R., *Ventilator graphics and respiratory mechanics in the patient with obstructive lung disease.* Respir Care, 2005. 50(2): p. 246-61; discussion 259-61.

37. Harris, R.S., D.R. Hess, and J.G. Venegas, *An objective analysis of the pressure-volume curve in the acute respiratory distress syndrome.* Am J Respir Crit Care Med, 2000. 161(2 Pt 1): p. 432-9.

38. Maggiore, S.M., J.C. Richard, and L. Brochard, *What has been learnt from P/V curves in patients with acute lung injury/acute respiratory distress syndrome.* Eur Respir J Suppl, 2003. 42: p. 22s-26s.

39. Venegas, J.G., R.S. Harris, and B.A. Simon, *A comprehensive equation for the pulmonary pressure-volume curve.* Journal of Applied Physiology, 1998. 84(1): p. 389-95.

40. Hantos, Z., B. Daroczy, B. Suki, S. Nagy, and J.J. Fredberg, *Input impedance and peripheral inhomogeneity of dog lungs.* Journal of Applied Physiology, 1992. 72(1): p. 168-78.

41. Bates, J.H.T., R. Farré, C.G. Irvin, and Z. Hantos, *Oscillation Mechanics of the Respiratory System.* Compr Physiol 2011. 1(2): p. 1233-1272.

42. Pauwels, R.A., A.S. Buist, P.M. Calverley, C.R. Jenkins, and S.S. Hurd, *Global strategy for the diagnosis, management, and prevention of chronic obstructive pulmonary disease. NHLBI/WHO Global Initiative for Chronic Obstructive Lung Disease (GOLD) Workshop summary.* Am J Respir Crit Care Med, 2001. 163(5): p. 1256-76.

43. Thurlbeck, W.M., *Pathophysiology of chronic obstructive pulmonary disease.* Clin Chest Med, 1990. 11(3): p. 389-403.

44. Barnes, P.J. and R.A. Stockley, *COPD: current therapeutic interventions and future approaches.* Eur Respir J, 2005. 25(6): p. 1084-106.

45. Ito, S., E.P. Ingenito, S.P. Arold, H. Parameswaran, N.T. Tgavalekos, K.R. Lutchen, and B. Suki, *Tissue heterogeneity in the mouse lung: effects of elastase treatment.* Journal of Applied Physiology, 2004. 97(1): p. 204-12.

46. Ito, S., E.P. Ingenito, K.K. Brewer, L.D. Black, H. Parameswaran, K.R. Lutchen, and B. Suki, *Mechanics, nonlinearity, and failure strength of lung tissue in a mouse model of emphysema: possible role of collagen remodeling.* Journal of Applied Physiology, 2005. 98(2): p. 503-11.

47. Dykstra, B.J., P.D. Scanlon, M.M. Kester, K.C. Beck, and P.L. Enright, *Lung volumes in 4,774 patients with obstructive lung disease.* Chest, 1999. 115(1): p. 68-74.

48. Vulterini, S., M.R. Bianco, L. Pellicciotti, and A.M. Sidoti, *Lung mechanics in subjects showing increased residual volume without bronchial obstruction.* Thorax, 1980. 35(6): p. 461-6.

49. Zamel, N., J. Hogg, and A. Gelb, *Mechanisms of maximal expiratory flow limitation in clinically unsuspected emphysema and obstruction of the peripheral airways.* Am Rev Respir Dis, 1976. 113(3): p. 337-45.

50. D'Armiento, J., S.S. Dalal, Y. Okada, R.A. Berg, and K. Chada, *Collagenase expression in the lungs of transgenic mice causes pulmonary emphysema.* Cell, 1992. 71(6): p. 955-61.

51. Mahadeva, R. and S.D. Shapiro, *Chronic obstructive pulmonary disease * 3: Experimental animal models of pulmonary emphysema.* Thorax, 2002. 57(10): p. 908-14.

52. Snider, G.L., E.C. Lucey, and P.J. Stone, *Animal models of emphysema.* Am Rev Respir Dis, 1986. 133(1): p. 149-69.

53. Tuder, R.M., S. McGrath, and E. Neptune, *The pathobiological mechanisms of emphysema models: what do they have in common?* Pulm Pharmacol Ther, 2003. 16(2): p. 67-78.

54. Bellofiore, S., D.H. Eidelman, P.T. Macklem, and J.G. Martin, *Effects of elastase-induced emphysema on airway responsiveness to methacholine in rats.* Journal of Applied Physiology, 1989. 66(2): p. 606-12.

55. Jeffery, P.K., *Remodeling in asthma and chronic obstructive lung disease.* Am J Respir Crit Care Med, 2001. 164(10 Pt 2): p. S28-38.

56. Collie, D.D., N. McLean, J.M. Sallenave, A. Baker, R. Blundell, E. Milne, S. Rhind, and C. Woodall, *Local lung responses following endobronchial elastase and lipopolysaccharide instillation in sheep.* Int J Chron Obstruct Pulmon Dis, 2006. 1(2): p. 189-99.

57. Lucey, E.C., R.H. Goldstein, P.J. Stone, and G.L. Snider, *Remodeling of alveolar walls after elastase treatment of hamsters. Results of elastin and collagen mRNA in situ hybridization.* Am J Respir Crit Care Med, 1998. 158(2): p. 555-64.

58. Hantos, Z., R.A. Collins, D.J. Turner, T.Z. Janosi, and P.D. Sly, *Tracking of airway and tissue mechanics during TLC maneuvers in mice.* Journal of Applied Physiology, 2003. 95(4): p. 1695-705.

59. Van de Woestijne, K.P., H. Franken, M. Cauberghs, F.J. Landser, and J. Clement, *A modification of the forced oscillation technique.* In: 28th Int Cong of Physiol Sci. Budapest, Hungary: Akademiai Kiado, 1981: p. 655-660.

60. Brown, R.H., D.M. Walters, R.S. Greenberg, and W. Mitzner, *A method of endotracheal intubation and pulmonary functional assessment for repeated studies in mice.* Journal of Applied Physiology, 1999. 87(6): p. 2362-5.

61. DuBois, A.B., S.Y. Botelho, G.N. Bedell, R. Marshall, and J.H. Comroe, Jr., *A rapid plethysmographic method for measuring thoracic gas volume: a comparison with a nitrogen washout method for measuring functional residual capacity in normal subjects.* J Clin Invest, 1956. 35(3): p. 322-6.

62. Janosi, T.Z., A. Adamicza, G.R. Zosky, T. Asztalos, P.D. Sly, and Z. Hantos, *Plethysmographic estimation of thoracic gas volume in apneic mice.* Journal of Applied Physiology, 2006. 101(2): p. 454-9.

63. Hantos, Z., F. Petak, A. Adamicza, T. Asztalos, J. Tolnai, and J.J. Fredberg, *Mechanical impedance of the lung periphery.* Journal of Applied Physiology, 1997. 83(5): p. 1595-601.

64. Alencar, A.M., S.P. Arold, S.V. Buldyrev, A. Majumdar, D. Stamenovic, H.E. Stanley, and B. Suki, *Physiology: Dynamic instabilities in the inflating lung.* Nature, 2002. 417(6891): p. 809-11.

65. Forgacs, P., *Breath sounds.* Thorax, 1978. 33(6): p. 681-3.

66. Suki, B., K.R. Lutchen, and E.P. Ingenito, *On the progressive nature of emphysema: roles of proteases, inflammation, and mechanical forces.* Am J Respir Crit Care Med, 2003. 168(5): p. 516-21.

67. Ito, S., E. Bartolak-Suki, J.M. Shipley, H. Parameswaran, A. Majumdar, and B. Suki, *Early emphysema in the tight skin and pallid mice: roles of microfibril-associated glycoproteins, collagen, and mechanical forces.* Am J Respir Cell Mol Biol, 2006. 34(6): p. 688-94.